UNIVERSITY OF CALIFORNIA
RIVERSIDE

Data-Driven Analysis of Convergence Bidding in Electricity Markets

A Dissertation submitted in partial satisfaction
of the requirements for the degree of

Doctor of Philosophy

in

Electrical Engineering

by

Ehsan Aliakbari Samani

June 2022

Dissertation Committee:

Dr. Hamed Mohsenian-Rad, Chairperson
Dr. Matt Barth
Dr. Evangelos Papalexakis

The Dissertation of Ehsan Aliakbari Samani is approved:

Committee Chairperson

University of California, Riverside

Acknowledgments

I am grateful to my advisor Dr. Hamed Mohsenian-Rad, whose help and guidance made this dissertation a reality. Many thanks to Dr. Matt Barth, Dr. Evangelos Papalexakis for their great feedback and being in my dissertation committee.

This work was supported in part by the National Science Foundation (NSF) and California Energy Commission (CEC) grants. The contents of this dissertation in Chapters 1, 2, and 3 include reprints of the material that are appeared in the following publications:

- **E. Samani**, M. Kohansal and H. Mohsenian-Rad, "A Data-Driven Convergence Bidding Strategy Based on Reverse Engineering of Market Participants Performance: A Case of California ISO," accepted for publication in IEEE Transactions on Power Systems.

- **E. Samani** and H. Mohsenian-Rad, "A Data-Driven Study to Discover, Characterize, and Classify Convergence Bidding Strategies in California ISO Energy Market," in Proc. of IEEE PES Innovative Smart Grid Technologies Conference (ISGT), Washington, DC, 2021.

- **E. Samani** and H. Mohsenian-Rad, "Understanding Convergence Bids During Blackouts: Analytical Results and Real-World Implications," under review in IEEE Transactions on Power Systems.

Furthermore, Chapter 4 includes summaries of the following collaborative efforts:

- M. Kohansal, **E. Samani** and H. Mohsenian-Rad, "Understanding the Structural Characteristics of Convergence Bidding in Nodal Electricity Markets," in IEEE Transactions on Industrial Informatics, vol. 17, no. 1, pp. 124-134, Jan. 2021.

- **E. Samani** et al., "Anomaly Detection in IoT-Based PIR Occupancy Sensors to Improve Building Energy Efficiency," 2020 IEEE Power Energy Society Innovative Smart Grid Technologies Conference (ISGT), 2020.

To my parents for all the support.

ABSTRACT OF THE DISSERTATION

Data-Driven Analysis of Convergence Bidding in Electricity Markets

by

Ehsan Aliakbari Samani

Doctor of Philosophy, Graduate Program in Electrical Engineering
University of California, Riverside, June 2022
Dr. Hamed Mohsenian-Rad, Chairperson

Convergence bidding is a mechanism in two-settlement electricity markets to reduce the price gap between the day-ahead market (DAM) and the real-time market (RTM). It also provides opportunities for market participants to arbitrage on the difference between the DAM locational marginal prices (LMPs) and the RTM LMPs. Two technical subjects related to convergence bids (CBs) are studied in this dissertation: 1) Given the fact that CBs have a significant impact on the operation of electricity markets, it is important to understand how market participants strategically select their CBs in real-world. This open problem is addressed in this dissertation by developing a data-driven reverse engineering method which results in identifying three main clusters of CB strategies in the California electricity market. Based on the lessons learned from the existing real-world strategies, a new CB strategy is proposed. We show through case studies that the performance of the proposed new strategy outperforms the most lucrative market participants in the California electricity market. 2) The operation and impact of CBs during blackouts are also investigated in this dissertation. The amount of load shedding is modeled as a function of the

amount of the cleared CBs. The sign of the slope of this function is proposed as a metric to determine if a CB exacerbates or heals the power outages. It is proved mathematically that, when there is no congestion in the DAM, the metric is always positive. Using numerical case studies, we show that, not only when there is no congestion, but also most often when there is congestion, the introduced metric is positive. The engineering implications of these results are discussed. Furthermore, the impact of load shedding on the profit of CBs is also analyzed to draw a complete picture in this analysis. It is shown that load shedding usually creates advantage for supply CBs and disadvantage for demand CBs in terms of their profit. The real-world California market data during the blackouts in August 2020 is also analyzed. It is shown that the decision to suspend CBs during this event matches the results that are obtained in this dissertation.

Contents

List of Figures

List of Tables

Chapter 1

Introduction

1.1 Overview of Electricity Markets

The concept of electricity markets in power system started with the deregulation of many electric utility companies world-wide which forced them to change their ways of doing business, from vertically integrated mechanisms to open market systems. Before deregulation, utility companies used to own the distribution network, the transmission network, and the generation units. In the United States, the Federal Energy Regulatory Commission (FERC) enacted Order 888 in 1996, a legal framework to increase competition in the U.S. wholesale electricity markets by promoting open access to the transmission networks. After deregulation of power systems, electricity markets are being operated by nonprofit organizations named Independent System Operator (ISO). Fig. 1.1 shows the current available ISOs in North America. Out of nine ISOs in North America, seven of them are located in the United States. The electricity markets running by the ISOs in

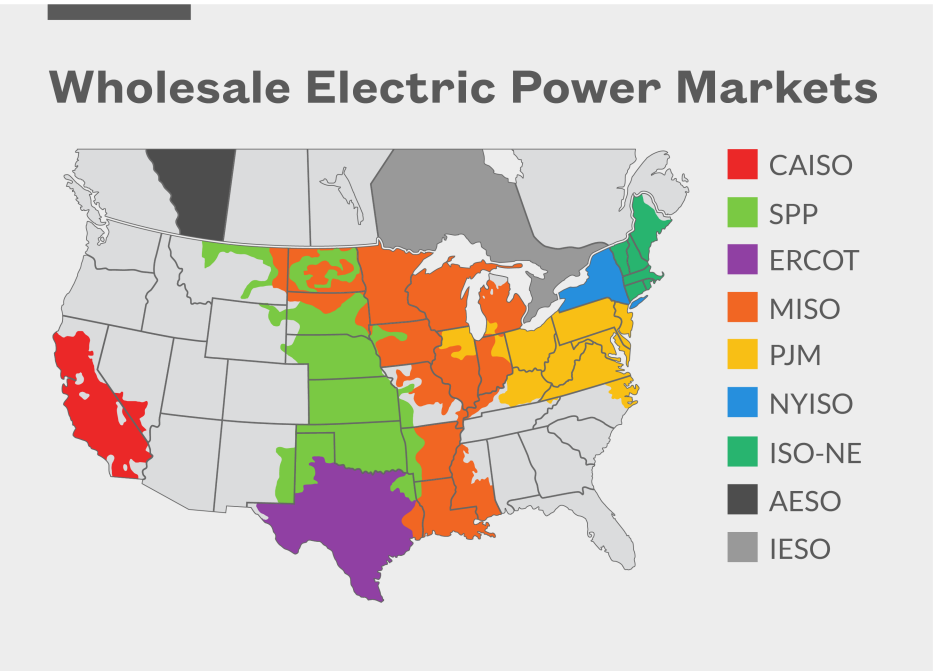

Figure 1.1: Available electricity markets operated by the ISOs in North America [1].

the United States have multiple steps. Day ahead markets (DAMs) and real time markets (RTMs) are the common steps between all the ISOs in the United States.

In the DAM, market participants submit their bids one day in advance. This market is only financially binding and not physically binding, i.e., market participants are not obligated to provide or consume the scheduled energy in the DAM. As a result, other than the physical market participants, virtual market participants with no physical asset can also participate in this market. The DAM provides an opportunity for both market participants and the ISOs to have a schedule and better planning for the next upcoming market day. The benefit of participating in the DAM for market participants is that they can trade in this market one day in advance with less volatility in the energy price.

In the RTM which usually happens a few minutes before the actual delivery, only the physical generation units can participant. In this market, the ISOs use their most updated load forecasting to make sure there would be enough available power for demand units at the time of delivery. If the output of a generator needs to be increased in the RTM compare to its schedule in the DAM, the additional generation will be paid based on the RTM prices while its DAM schedule will be paid based on the DAM prices. Similarly, if the output of a generator decreases in the RTM compare to its schedule in the DAM, this generator will be charged for the amount of reduction based on the RTM prices.

1.2 Convergence Bidding in Electricity Markets

Convergence bidding, a.k.a., virtual bidding, is a financial market mechanism that is used by the ISOs in two-settlement wholesale electricity markets to reduce the price gap between the DAM and the RTM in order to increase market efficiency [2, 3]. As it is mentioned in the last section, convergence bids (CBs) can participate in the DAM. A supply CB is a bid to sell energy in DAM without any obligation to produce energy in the RTM. A demand CB is a bid to buy energy in DAM without any obligation to consume energy in the RTM [4]. While CBs are virtual, i.e., only financial and not physical, they are cleared in the DAM together with physical supply and demand bids. If a supply CB is cleared in the DAM, then the bidder is credited at the DAM price and charged at the RTM price; because CB is not submitted to the RTM. If a demand CB is cleared in the DAM, then the bidder is charged at the DAM price and credited at the RTM price. In both cases, the *difference* between the earning or loss is paid to the convergence bidder. The process of clearing CBs

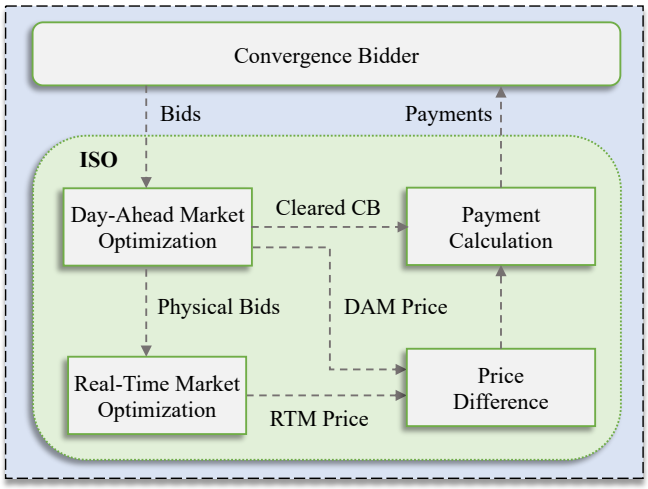

Figure 1.2: The process of clearing CBs in wholesale electricity markets.

and the related payment calculation is outlined in Fig. 1.2, [4]. The payment is calculated by multiplying the cleared amount of energy by the *difference* between the DAM locational marginal price (LMP) and the RTM LMP.

California ISO and all the other ISOs in the United States utilize convergence bidding in their market [5, 6]. Some of the potential advantages that are identified for supporting CBs include the following: improving the efficiency of the day-ahead commitment and energy schedules, reducing the cost of hedging, allowing for efficient settlement of financial transmission right, and making it advantageous for parties to utilize the liquidity provided in the market [7]. CBs can also affect the integration of renewable energy resources and demand response resources in electricity markets, e.g., see [8–10]. Aside from the mentioned potential advantages for convergence bidding, in Chapter 3, we show that CBs can have some serious disadvantages as well. We show how they can impact the amount of load shedding during an outage condition in the power systems.

1.3 Literature Review

Despite the fact that CBs are widely adopted by the ISOs in recent years, the current literature is still limited when it comes to the analysis and understanding of convergence bidding. The existing literature in this area can be broadly divided into three groups:

1.3.1 Impact of CBs on the market efficiency

In the first group, there are papers that study the impact of CBs on the efficiency and the operation of electricity markets [4, 11–26]. In [4], a method is proposed to identify under what theoretical conditions a CB results in price divergence, instead of price convergence. In [11], the author analyze the impact of convergence bidding on the Midcontinent Independent System Operator (MISO) electricity market. It is discussed in this paper that CBs does not necessarily eliminate the market power activities. The impact of convergence bidding on the efficiency of the California ISO market and impact on price convergence is studied in [12] and also in [17]. In [13] the impact that virtual bidding has on price volatility in the New York ISO market is examined. Virtual bidding is found in this paper to be associated with reduced volatility in both the DAM and the RTM. The authors in [14] develop a two-settlement market model by following a data-driven approach. The main results in this study convey the implication that introducing more qualified virtual bidders into the market help the convergence of the price difference between the DAM and the RTM. The study in [15] indicates that virtual bidding is associated with lower premiums in off-peak or near-off-peak hours while it is associated with higher premiums during peak

hours. By adopting a game-theoretic model of virtual bidding, the study in [18] shows that as the number of virtual bidders increases, the equilibrium market outcome tends to the socially optimal DAM schedule, and prices converge between the DAM and the RTM. In [22], the authors seek to provide empirical evidence to evaluate the effectiveness of virtual transactions in helping converge market prices using simulations of the PJM wholesale energy market clearing process. Results show that some virtual transactions do support the convergence of the DAM and the RTM prices while others do not.

1.3.2 Manipulation of market through CBs

As the second group of papers in this area, there are some studies in the literature that are concerned with the potential to manipulate the wholesale electricity market by using CBs [27–33]. The authors in [27] present a model that distinguishes between legitimate market participation that increases overall market efficiency and manipulative behavior that distorts markets and reduces efficiency. It is discussed in this study that intentional uneconomic trading of virtual bids to trigger a manipulation causes the divergence of the DAM and the RTM nodal prices and thus creates market distortions and inefficiencies. In [28], an equilibrium model is developed to study the cross-product manipulation in financial transmission right (FTR) and two-settlement energy markets. The concept of cyber attacks in wholesale electricity markets with virtual bidding activities is analyzed in [31]. A framework is proposed to evaluate the economic profit of an attacker who conducts a topology data attack using CBs.

1.3.3 Bidding strategies of CBs

The papers in the third group develop and study the bidding strategy of CBs in the electricity markets. Some of the related papers include [34–42]. In [34], an online learning algorithm is proposed to maximize the cumulative payoff over a finite number of CB trading sessions. In [36], a stochastic optimization model is proposed to place CBs under different risk management scenarios. In [37], a bi-level CB optimization problem is proposed, where the upper-level problem aims to maximize the profit for the convergence bidder and the lower-level is the economic dispatch problem. In [38] convergence bidding is used to help photovoltaic solar power producers improve their profits and manage their risk. A stochastic optimization model is established in this study to co-optimize the profits of solar power offering and convergence bidding, where the seasonal autoregressive integrated moving average (SARIMA) model is used for scenario generation and Conditional Value at Risk (CVaR) is used as a risk measure. The study in [39] proposes a risk-constrained bi-level optimization model for convergence bidding strategy. In this model, uncertainties related to the other market participants' bids and the RTM prices are modeled through scenarios. The authors in [40] propose a bi-level stochastic optimization model for joint physical demand bidding and convergence bidding, for a strategic retailer in the short-term electricity market. In [41], different types of convergence bidding strategies that are currently used by market participants in California ISO is analyzed. This work develop a data-driven reverse engineering which results in identifying three main clusters of CB strategies in the California ISO market.

1.4 Research Problems

In this dissertation, we are trying to answer a series of research questions regarding convergence bidding in two parts. In the first part, we want to understand the characteristics and the strategy of the real-world CB market participants and learn from their strategies. In this part, we focus on the following research question:

1) What are the characteristics of the submitted CBs in real-world power markets? 2) How do market participants shape their CB strategy, in particular with respect to the choice of their price bids? 3) How does the reality of the CB strategies in the California ISO market match the existing literature in this field? 4) What are the most common strategies that are used by the CB market participants in the California ISO market? 5) Is it possible to learn from the current CB strategies in the California ISO market and propose a new strategy that can significantly outperform them? 6) Could a CB strategy that is seemingly unprofitable comprise part of an enhanced new composite bidding strategy?

In the second part, we are looking to examine the operation and the impact of convergence bids during major *blackouts*. Accordingly, in this part, we seek to answer the following research questions:

1) Despite being a financial tool, does convergence bidding have an impact on the required amount of load shedding during blackouts? 2) If the answer is 'yes', then how can we understand and explain such impact and its extent and circumstances? 3) Conversely, is there a relationship between load shedding and the profit of supply CBs and demand CBs during power outages? 4) Can we use the answers to the above questions to explain why the California ISO decided to entirely suspend CBs for four days during the blackouts

which were caused by a major heat-wave in August 2020? 5) What else can we learn from this real-world incident in California, such as with respect to the profitability and impact of CBs during major power outages?

Chapter 2

A Data-Driven Convergence Bidding Strategy Based on Reverse Engineering of Market Participants' Performance

2.1 Introduction

Understanding how market participants *strategically* select their CBs in *real-world* electricity markets is the focus of this chapter and its corresponding papers in [41, 42]. We address this open problem with a focus on the electricity market that is operated by the California ISO. In this regard, we use the publicly available electricity market data *to learn, characterize, and evaluate* different types of convergence bidding *strategies* that

are currently used by market participants. Our analysis includes developing a *data-driven reverse engineering* method that we apply to three years of real-world California ISO market data. Our analysis involves feature selection and density-based data clustering. It results in identifying *three main clusters* of CB strategies in the California ISO market. Different characteristics and the performance of each cluster of strategies are analyzed. Interestingly, we unmask a common real-world strategy that does *not* match any of the existing strategic convergence bidding methods in the literature. Next, we build upon the lessons learned from the advantages and disadvantages of the existing real-world strategies in order to propose a new CB strategy that can significantly *outperform* them. Our analysis includes developing a new strategy for convergence bidding. The new strategy has three steps: net profit maximization by capturing price spikes, dynamic node labeling, and strategy selection algorithm. We show through case studies that the annual net profit for the most lucrative market participants can increase by over 40% if the proposed convergence bidding strategy is used.

2.1.1 Summary of Contributions and Discoveries

While the basic principles of convergence bidding are studied in the academic literature and industry reports, there is currently a gap in this field about understanding the strategy and behavior of CB market participants in real-world electricity markets. This is a critical subject because the way that market participants select their CBs can ultimately shape the impact of CBs on electricity markets. Addressing this open problem is the focus of this chapter. Accordingly, the main discoveries and contributions in this chapter are as follows:

- Three years of real-world market data from the California ISO market are investigated to understand the behavior of CB market participants. The analysis is comprehensive; it looks into all the submitted CBs, D-LMPs, R-LMPs, and the net cleared CBs. The convergence bidders that are most present in the market are identified based on different metrics; and their CBs are analyzed in terms of the number of submitted CBs, the number of participated locations, the type of submitted CBs, the number of steps for the submitted CBs, and the quantity of the submitted CBs in MWh.

- The *features* for the strategy of the submitted CBs are extracted; and by using a density-based clustering algorithm, *three main clusters* of CB strategies are identified. The characteristics and the performance of each identified cluster of strategies are analyzed and some of their *advantages* and *disadvantages* are investigated. Next, the identified strategies are *reverse engineered*, i.e., their key steps are identified such that we can implement them for a market participant. The purpose of this reverse engineering task is two-fold. First, it can shed light on *how* CB market participants behave. This by itself is an important study and the results can be insightful to ISOs and policy makers. Second, it serves as means for us to develop a *new* and better convergence bidding strategy based on what we learn from the current state of practice.

- Our analysis also unmasks two interesting discoveries. First, one of the most common real-world CB strategies in the California ISO market does *not* match any of the strategic convergence bidding methods that currently exist in the research literature. Second, most of the exciting papers in the research literature are focused on one of

the CB strategies that is *less* common in practice among the CB market participants in the California ISO market.

- A new comprehensive convergence bidding strategy is proposed to utilize the identified reverse engineered strategies based on their advantages and disadvantages under various market conditions. To the best of our knowledge, this is the first composite CB strategy that is proposed in the literature. It is also the first CB strategy that is obtained by reverse engineering of existing real-world CB strategies. The proposed strategy comprises *three steps*: net profit maximization by capturing price spikes, dynamic node labeling, and strategy selection. We show that the annual profit for the most lucrative market participant in the California ISO market can increase by 43%; if the proposed bidding strategy is used.

2.2 Overview of the Real-World CB Market Participation Data in the California ISO

In this section, we provide an overview of the CB market participation in the California ISO electricity market based on the real-world market data. All the raw data in this study are available in [43]. The analysis in this section will address Research Question 1. It will also set the stage for the data-driven reverse engineering work in Section 2.3.

2.2.1 Analyzing the Market Data

Three years of market data from the California ISO electricity market, during 2017, 2018, and 2019, are analyzed.

A CB that is submitted to the California ISO electricity market must contain four pieces of information as follows: i) step-wise quantities (MWh), ii) step-wise prices[1] ($/MWh), iii) the type of the CB, which can be either a demand CB or a supply CB, and iv) the nodal location of the CB. In the California ISO electricity market, the CB market participants can submit up to ten steps of quantity and price pairs in each bid. It should be mentioned that, throughout this chapter, if a CB is multi-step, then the maximum quantity of the different steps of the same submitted CB is considered as its *quantity*.

In this study, we focused on the aggregated pricing nodes (APnodes) in the California ISO market. As defined by the California ISO, an APnode is a trading hub, a load aggregation point, or any group of multiple pricing nodes (Pnodes) [44]. The reason that APnodes are the focus of this study is that, most of the submitted CBs in the California ISO market are at the APnodes. There is no practical advantage to look into any higher locational resolution beyond APnodes. With over two thousand APnodes across the state of California, focusing on the APnodes in this study already required handling a huge amount of real-world market data. Accordingly, we examined a total of 2265 APnodes; out of which a total of 475 APnodes hosted at least one CB at any time during the three-year period of this study. On average, a total of 387 APnodes hosted at least one CB during each month.

[1]Throughout this chapter, we refer to the price bids, which are expressed in $/MWh, as the *price components* or the *price values* of the convergence bids.

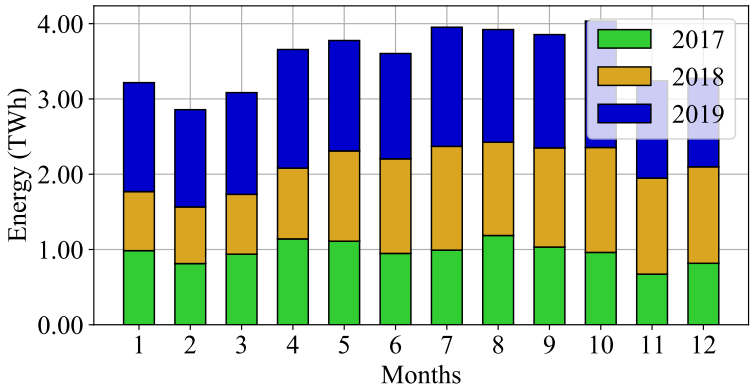

Figure 2.1: Total monthly amount of cleared energy by CBs for each year.

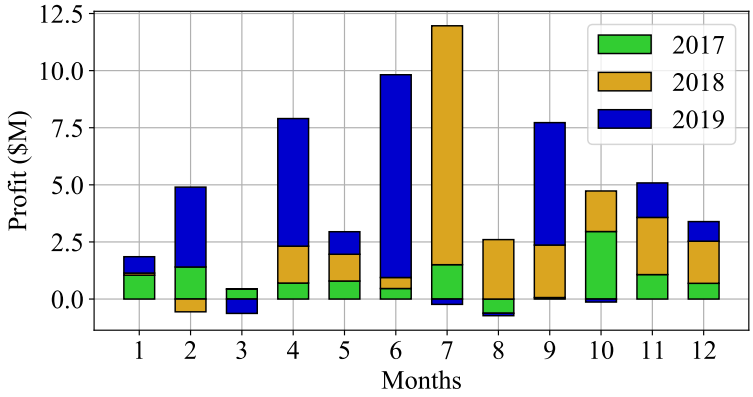

Figure 2.2: Total monthly net profit by convergence bidders for each year.

The total number of *market participants* that ever submitted a CB during the three-year period of this study was 101, with a monthly average of 52 market participants. The total profit that was earned by all the market participants in the CB market during this period was $61 million. Out of the 101 convergence bidders, 74 of them made money, i.e., had a *net positive profit*. Fig. 2.1 shows the total monthly amount of cleared energy at each year for the convergence bidders, and Fig. 2.2 shows the monthly net profit that all the convergence bidders earned during this period of study. Note that, notation $M

means $1,000,000. Interestingly, there were months that the market participants had an overall loss, i.e., *net negative profit* as the outcome of their convergence bidding. Another interesting observation is that even though the net profit fluctuated significantly across different months, the amount of cleared CB was about the same in each month.

As it is already widely discussed in the literature, there is a direct relationship between the CB market participants' ability to earn profit, and the advantages that convergence bidding can provide to the society from the system viewpoint. In particular, as discussed in the ISO reports, such as in [5, 6], if the CB market participants make profit, then their CBs also help closing the gap between D-LMPs and R-LMPs. Closing such gap results in several benefits to the system, such as [5, 6]: 1) Lowering the costs due to more efficient day-ahead commitment, 2) Improving the grid operations and reliability, 3) Market power mitigation, 4) Increasing the market liquidity, 5) Promoting the competition between market participants. The above mentioned fact in the ISO reports, that a profitable CB helps with achieving price convergence and its advantages, is also proved mathematically in [4].

2.2.2 Identifying the Most Present Convergence Bidders

In this work, although we analyze *all* the submitted CBs in the California ISO market, we scrutinize only the "most present" convergence bidders for the purpose of extracting their convergence bidding strategies. The most present CB market participants can be defined based on different metrics: 1) their high share in the market in terms of the number of submitted CBs; 2) their high share in the market in terms of the number of cleared CBs; 3) their high share in the market in terms of the total amount of quantity of

the submitted CBs in MWh; 4) their high share in the market in terms of the total amount of quantity of the cleared CBs in MWh.

The process of selecting the most present market participants is summarized in Table 2.1. For each metric, we calculated the share (in percentage) of all the CB market participants according to that particular metric. We then sorted the list of market participants based on each metric, and accordingly selected the market participants with the 10 highest shares in the market according to each metric. The 10 selected market participants for each metric are marked in Table 2.1 by gray shaded areas. There are exactly 10 market participants with gray shaded areas in each column. Next, we combined the four lists from the four metrics. Due to the overlaps between the lists for the four metrics, this analysis results in identifying a total of 20 market participants as the ones that are "most present" in the CB market. At this stage, we assigned *Alias IDs* to the selected market participants, as denoted by 1 to 20. As it is mentioned before, the total number of CB market participants that ever submitted a CB during the period of this study is 101. The reason for choosing the 10 highest shares of each list of metrics is to select all market participants that *one way or another* have some considerable presence in the market, then we scrutinize the selected market participants. Note that, each of the 20 selected market participants has a considerable presence in the market based on *at least* one of the four metrics. As we can see in the last row in Table 2.1, the identified 20 most present market participants in the above process accounted for 72% to 84% of the entire convergence bidding market, based on any of the four metrics that one can consider to define the share of the market participants.

Table 2.2 shows some basic information for each Alias ID that we previously identified in Table 2.1. We can make several preliminary observations, as we explain next.

Some of the identified convergence bidders placed CBs in almost all the locations that ever received CBs, such as Alias ID 4 that placed CBs in 95% of locations that hosted at least one CB at any time during the three-year period of this study. Some other convergence bidders placed CBs in only a few locations, such as Alias ID 20 that placed CBs in less than 1% of the locations. Most of these 20 convergence bidders with considerable presence submitted both supply and demand bids, but some of them, such as Alias ID 17 and Alias ID 20, submitted supply CBs more than demand CBs, or vice versa.

Based on the average value for the number of steps for the cleared CBs, some market participants always submitted single step bids, while some others used multiple steps in their CBs. Finally, the average quantity of the cleared CBs varies from about 2 MWh to 156 MWh which shows a different amount of investment and available credit between market participants.

2.3 Data-Driven Reverse Engineering of the Convergence Bidding Strategies

In this section, first, we will extract different quantitative *features* to characterize the convergence bidding strategies of the market participants based on the raw market data that we introduced in Section 2.2. After that, we will use the extracted features to *cluster* the submitted CBs into three clusters of strategies. Finally, the performance of the clusters

of strategies will be compared. By going through these steps, the convergence bidding strategies of the real-world market participants in the California ISO market will be *reverse engineered*. The benefit of this analysis is two-fold. First, an in-depth understanding of the CB strategies that are currently adopted by the real-world market participants is in its own right interesting from the view point of research and also to provide insights to ISOs. Second, by unmasking and reverse engineering the existing real-world CB strategies in the California ISO market, an enhanced and more profitable CB strategy is achieved, as we will see in Section 2.4.

2.3.1 Features for Cluster Identification

Recall from Section 2.2.1 that each submitted CB has three types of information: quantities, prices, and whether it is a demand CB or a supply CB. The pair of quantity and price can be submitted in one step or multiple steps. Accordingly, we introduce four different *features* for each submitted CB: 1) The price distance, i.e., the difference between the price bid in the submitted CB at a node and the average hourly D-LMP[2] at that node; 2) The correlation between the type of the submitted CB (demand or supply) at a node and the historical CBs at that node; 3) The number of steps in the submitted CB; 4) The type of node where the CB is submitted, i.e., whether the node is a regular APnode, i.e., it is *not* a Hub or a DLAP, or it is one of the major aggregated nodes in the California ISO market, i.e., it *is* a Hub or a DLAP.

[2]The average D-LMP is a fixed number for each hour and each node, as it is the mean value of the historical prices over a period of three years.

In this work, we seek to consider the key determinative features for the bidding strategy of the CB market participants. In our assessment, the selected features should have three main characteristics as follows. First, the selected feature should be built only based on the data that each market participant has access to by its own. For example, a feature that needs to include other market participants' bidding information is not considered in our features for the purpose of clustering. This is because each convergence bidder does not have access to the bidding data of other market participants. Second, the selected feature should not involve or depend on the information that is private to the market participant. It is not really a choice to not consider such private information; it is rather the nature of a study like ours that is based on analyzing real-world electricity market data. For example, each CB market participant has a "credit" with California ISO, which determines the maximum quantity of bids that the market participant can submit to the market. Such "credit" is not public data. Thus, the quantity of the submitted CB in MWh is not considered as a feature, because it is not clear whether the quantity of the bid is simply set based on the market participant's "credit" or it is a factor that is strategically selected by the market participant. Third, the selected feature should be built only based on the data that each market participant has access to *at the time of submitting* its bid to the California ISO market. For example, the same day LMPs are *not* known to the market participants at the time of submitting their bids, but the historical average of the LMPs for each location and each hour *is* known to them.

Fig. 4 shows the definition of the first feature for a multi-step supply CB and a multi-step demand CB. This feature is denoted by Δ. In this figure, the green horizontal

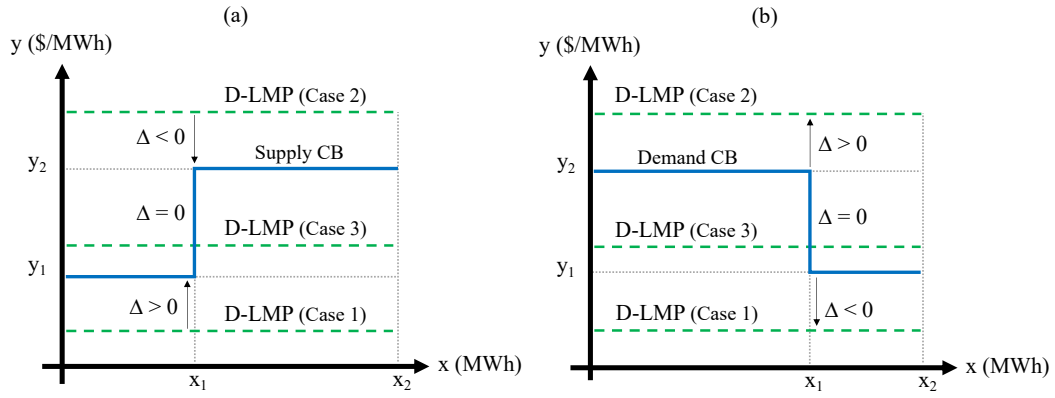

Figure 2.3: Demonstration of the first feature, i.e., Δ, which is the price distance of bid from average hourly D-LMP: a) in a supply bid; b) in a demand bid.

dashed line is the average hourly D-LMPs for the hour corresponding to a given CB. Three green lines show three possible different cases that will be explained in follow. First, consider a supply CB in sub-figure (a). Three cases can happen: 1) All the submitted price values in a given CB are higher than the average D-LMP. In other words, the entire piecewise linear function for the submitted CB is above the average D-LMP. In this case, $\Delta > 0$ and it is defined to be equal to the minimum price value in the submitted CB minus the average D-LMP. 2) All the submitted price values in a given CB are lower than the average D-LMP. In other words, the entire piecewise linear function for the submitted CB is below the average D-LMP. In this case, $\Delta < 0$ and it is defined to be equal to the maximum price value in the submitted CB minus the average D-LMP. 3) The average D-LMP is somewhere between the minimum and the maximum price values in the submitted CB. In other words, the average D-LMP has an intersection with the piecewise linear function for the submitted CB. In this case, $\Delta = 0$ and it is defined to be zero. Next, consider a demand CB in sub-figure (b). Again, three cases can happen, which can be defined similarly. The only difference is that, when it comes to a demand CB, in the first case, Δ is equal to the average

D-LMP minus the minimum price value in the submitted CB (not the other way around); and in the second case, Δ is equal to the average D-LMP minus the maximum price value in the submitted CB (not the other way around). In other words, the previously defined Δ should be multiplied by -1.

The second feature indicates whether the same type of CB, i.e. a supply CB or a demand CB, has been consistently used by a market participant at a nodal location. This feature is a number between 0 and 1. This feature indicates whether the type of the submitted CB is similar or dissimilar to the type of the CBs historically submitted by the same market participant at the same location. The value of this feature is close to 1, if the market participant consistently selects the same type of CB at the given node; and the new submitted CB also has the same type. The value of this feature is close to 0, if the market participant consistently selects the same type of CB at the given node; but the new submitted CB has a different type. Finally, the value of this feature is close to 0.5 if the market participant frequently changes the type of its submitted CBs at the given node; i.e., it submits a mix of both supply CBs and demand CBs. As an example, consider all the previous CBs that are submitted by a market participant at a node. Suppose 60% of the CBs are supply bids and 40% of the CBs are demand bids. If the current CB is a supply CB, then the second feature would be 0.6. If the current CB is a demand CB, then the second feature would be 0.4. In this work, a window of one year of historical data, i.e., the data over the previous year, is considered for calculating this feature.

The third feature is the number of steps in the submitted CB, which is an integer number between one and ten.

The fourth feature is driven by the fact that some market participants submit CBs *only* at the major aggregated nodes, in the California ISO market, i.e., at one or more of its three Hubs, namely NP15, SP15, and ZP26, or its three Default Load Aggregated Points (DLAPs), which include San Diego Gas and Electric (SDG&E), Pacific Gas and Electric (PG&E), and Southern California Edison (SCE). Importantly, these major aggregated nodes have *a higher level of predictability* for LMPs, compared to the regular APnodes. This feature somewhat incorporated two other candidate features, namely the LMP volatility and the LMP forecast accuracy of the node where the CB is submitted. In fact, higher volatility in LMP values directly results in less accuracy in forecasting the LMP values. This fourth feature is a binary number on whether or not the node is a major aggregated node. It should be noted that, in the California ISO market, the major aggregated nodes are among the APnodes.

2.3.2 Identified Convergence Bidding Clusters

Based on the introduced features in Section 2.3.1, next, we classify the submitted CBs by using the Hierarchical Density-Based Spatial Clustering of Applications with Noise (HDBSCAN) method. HDBSCAN is a robust clustering algorithm that can work with little or no parameter tuning [45]. The only parameter that needs to be tuned in this method is the minimum number of points in each cluster.

The data points in this analysis are the collection of all the submitted CBs over the three-year period of this study, which add up to 6.6 million CBs. The purpose of our clustering analysis is to gain insights from such a huge amount of data, such that we can identify the main convergence bidding strategies in the California ISO market. Accordingly,

our analysis is a hybrid of applying data-driven algorithms and manual inspection of the data-driven results. In the latter (i.e., manual) inspection, we examined the data-driven results with respect to the four features and we accordingly identified three clusters that can cover practically all the existing major convergence bidding strategies in the California ISO market during the period of this study. In this process, we combined artificial intelligence with human expertise to translate the bidding data to the most meaningful clusters. It should be mentioned that, the clustering in this analysis is done only once and it is done for the entire dataset in the period of this study. Our approach to involve both machine intelligence and human expertise, is very suitable for the purpose of this study which involves a huge amount of bidding data. The definition of each cluster and its work function is defined as follows:

CB Cluster 1 (Price-Forecasting Strategy): This strategy is the case where the CB market participant submits price bids that are *close* to the LMP values at the location where the CB is placed; making it evident that the market participant is trying to forecast the market prices at its bidding locations. For each hour of the next day, if the forecasted D-LMP is higher than R-LMP, then a supply CB is submitted. If the forecasted D-LMP is lower than R-LMP, then a demand CB is submitted. For a supply CB, the price values should be *less* than the forecasted D-LMP but *close* to it in order to avoid entering the market when D-LMP is unexpectedly low. Also, for a demand CB, the price values should be *more* than the forecasted D-LMP but *close* to it in order to avoid entering the market when D-LMP is unexpectedly high. As a result, in this cluster: 1) Δ is relatively small. 2) The correlation between the type of the submitted CB and those of the previous

CBs of the same market participant at the same location is often not close to 1, because the convergence bidder is trying to actively forecast the LMPs. As a result, the types of the CBs are selected according to the forecast results, and they can vary depending on the market conditions. 3) The number of steps for the submitted CB can be single or multiple, and this is *not* a determinative feature in this cluster of strategies. 4) The CB is mostly submitted in a major aggregated node, with a higher level of locational price predictability, because this strategy requires accurate forecasting of both D-LMP and R-LMP. However, in principle, it is possible that a market participant uses this strategy on regular APnodes, if they *can* achieve accurate LMP forecasts at that node.

CB Cluster 2 (Self-Scheduling Strategy): This strategy is the case where the CB market participant does not mean to calculate and submit a price bid, i.e., its CB is mainly about its quantity. It should be clarified that, in principle, all CBs in the California ISO market *must* include at least one price value. Thus, when a CB market participant follows a self-scheduling strategy, it still needs to include a price value in its CB. For a demand CB, the price value should be *much higher* than the expected D-LMP for that hour, i.e., the average D-LMP for that hour, such that the submitted CB is always cleared in the market. For a supply CB, the price value should be *much lower* than the expected D-LMP, such that the submitted CB is always cleared in the market. In both cases, i.e., whether the submitted CB is a demand bid or a supply bid, it would result in a large negative Δ. Importantly, as far as the price-forecasting is concerned, the self-scheduling strategy only needs a *rough forecast* about the *sign* of the difference between D-LMP and R-LMP in order to decide on whether to submit a supply CB or a demand CB. For each hour

of the next day, if the difference between D-LMP and R-LMP is expected to be *positive*, then a supply CB is submitted; and if such difference is expected to be *negative*, then a demand CB is submitted. As a result, in this cluster: 1) Δ is relatively large and negative. 2) The correlation between the type of the submitted CB and those of the previous CBs of the same market participant at the same location is often *not* close to 1, because the convergence bidder may submit different types of CBs based on the expected sign of the difference between D-LMP and R-LMP. 3) The submitted CB is *single* step. This is an important determinative feature in this cluster of strategies, because multi-step strategies cannot match the definition of self-scheduling bids. 4) The CB may be submitted at regular APnodes *or* at the major aggregated nodes.

CB Cluster 3 (Opportunistic Strategy): This strategy is the case where the CB market participant does not want to get involved in the difficulties of doing an accurate price forecast, yet it does not want to be as passive as in the self-scheduling strategy (as far as the selection of its price bid is concerned). Hence, the market participant takes a third option, which is somewhat opportunistic. In this strategy, the CB market participant always submits either a supply CB that has a price bid that is considerably higher than the D-LMPs, or a demand CB that has a price bid that is considerably lower than the D-LMPs. In this regard, the CB market participant waits for a *spike* in D-LMP to enter the market. As a result, the submitted bids are *not* cleared most of the time. They are cleared only occasionally, when there is a potential opportunity to make a considerable profit. Interestingly, this is a completely new CB strategy and it does not match any of the strategic convergence bidding methods that currently exist in the literature. Thus, we

will provide a detailed explanation about the application of this strategy in Section 2.4. In this cluster: 1) Δ is relatively large and positive. 2) The correlation between the type of the submitted CB and those of the previous CBs *is* often close to 1. 3) The number of steps for the submitted CB can be single or multiple, and it is *not* a determinative feature in this cluster. 4) The CB is almost always submitted at regular APnodes, but *not* at the major aggregated nodes. This is an important determinative feature in this cluster, because convergence bidders should find those nodes that have a potential for experiencing price spikes. Major aggregated nodes with high levels of predictability do not carry this characteristic.

The above three identified clusters and their introduced characteristics address Research Question 2.

The above analysis can also be used to address Research Question 3. Importantly, while CB Cluster 2 is *less* common among market participants, yet many of the existing papers in the literature *are* in fact focused on this strategy. Furthermore, CB Cluster 3 is a common strategy in the California ISO market, yet it does *not* match any of the strategic convergence bidding methods that currently exist in the literature. In fact, the strategy in CB Cluster 3 is currently used by several market participants, including Alias ID 1, which is the most active market participant in the California ISO market, in terms of the number of submitted CBs.

Another note to highlight is that the *same* market participant may have *different* strategies at *different* nodes. For example, consider the hourly value of the first feature (Δ) in Fig. 2.4 for the submitted CBs by Alias ID 5 in two *different* locations. As we can

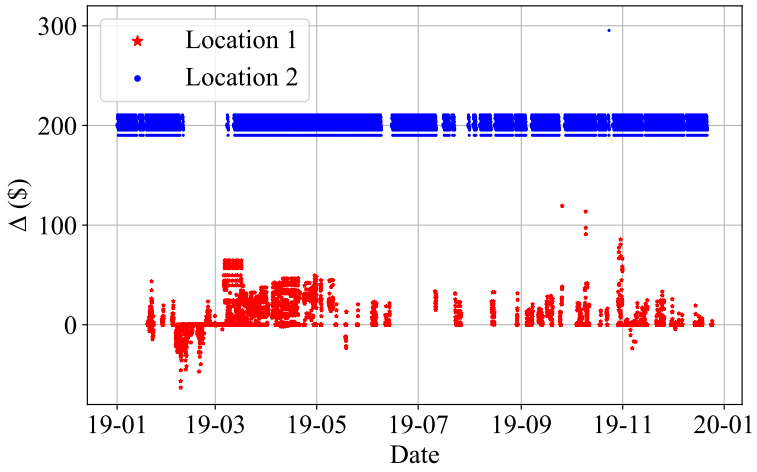

Figure 2.4: The first feature (Δ) for Alias ID 5 at two different locations during 2019. It is evident that this CB market participant uses two different bidding strategies as these two different locations.

see, there is a clear distinction between the strategies that Alias ID 5 chose at these two different locations.

An interesting observation is that, some of the CB market participants have clearly *changed* their strategy during the period of this study. For example, Fig. 2.5 shows the first introduced feature, i.e., the distance of the submitted price bids from the average D-LMPs, at each hour for Alias ID 6. We see that this market participant clearly changed its bidding strategy around February 2019. While its bidding strategy in 2018 mostly matches the Opportunistic Strategy, its bidding strategy in 2019 mostly matches the Price-Forecasting Strategy.

As a side note, no other market participant changed her convergence bidding strategy around the date that Alias ID 6 changed her strategy. Therefore, while we cannot

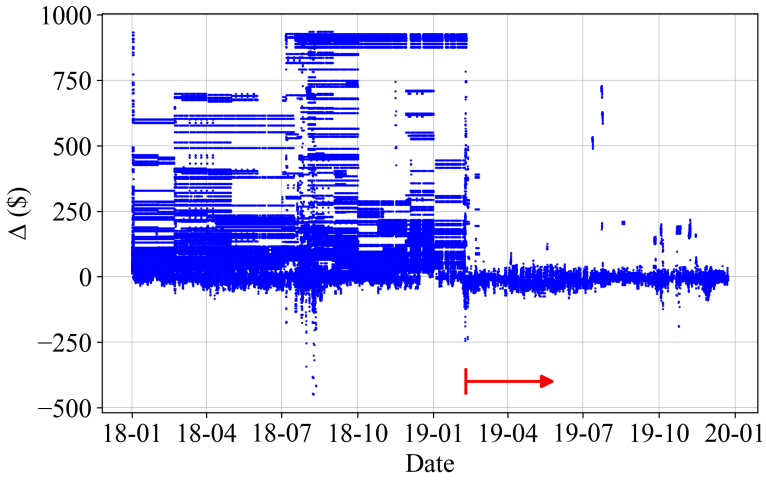

Figure 2.5: The first feature (Δ) at each hour for Alias ID 6 over a period of two years. It is evident that this CB market participant changed its bidding strategy in February 2019.

speculate on the reason for Alias ID 6 to change her strategy, it is more likely that the change was due to Alias ID 6's own internal factors than a change in the system.

2.3.3 Performance Comparison among Identified Strategies

To complete the reverse engineering task, next, we evaluate the performance of each CB cluster to understand the advantages and the disadvantages of different CB strategies. Two metrics are used to assess and compare the performance of different CB clusters. The first metric is the *cleared-to-submitted-ratio* (CSR), which is the percentage of the submitted CBs that are cleared in the market for each market participant:

$$\text{CSR} = \frac{\text{Number of Cleared CBs}}{\text{Number of Submitted CBs}} \times 100. \tag{2.1}$$

The second metric is the *loss-to-profit-ratio* (LPR), which can help capture the level of loss compared to the level of profit. This metric is defined as follows:

$$\text{LPR} = \frac{\text{Total Loss}}{\text{Total Profit}} \times 100. \tag{2.2}$$

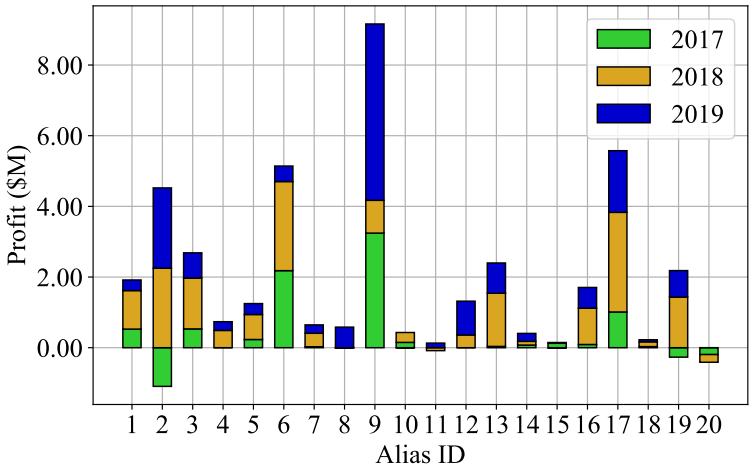

Figure 2.6: Total yearly amount of earned/lost profit by each Alias ID.

A lower CSR indicates that only a small portion of the submitted CBs for a given market participant at a given node is cleared. A lower LPR indicates that the cleared CBs of a given market participant at a given node resulted in more profits than losses. Together, CSR and LPR draw a clear picture about the portion of the CBs that are cleared and the circumstances in terms of loss versus profit for the cleared CBs. Note that, we do *not* consider the total net profit as a comparison factor, because it depends on each market participant's credit in the California ISO market, which limits the quantity of their submitted CBs.

The CSR is listed in Table 2.3 for all the identified Alias IDs. For each CB cluster, the performance of one representative market participant is considered for benchmarking.

Alias ID 9, which is the *most lucrative* CB market participant in the California ISO market (Fig. 2.6), mostly used the Price-Forecasting Strategy on the major APnodes. Fig. 2.7 shows the hourly per unit profit ($/MWh) for Alias ID 9 in one of the three DLAPs

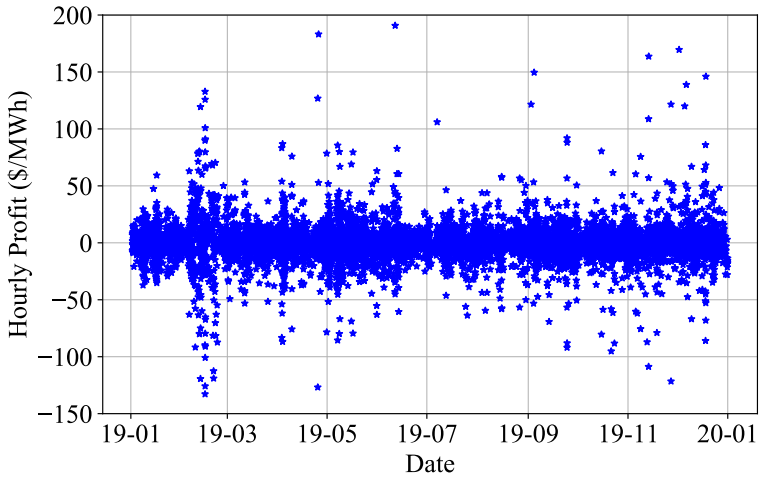

Figure 2.7: Hourly profit for Alias ID 9 using the Price-Forecasting Strategy at a DLAP.

using the Price-Forecasting Strategy. As we can see, there are many hours with a loss for the submitted CBs by this market participant. For these CBs, CSR and LPR are 86.43% and 73.62%, respectively. These values show that most of the submitted CBs by Alias ID 9 are cleared, and some of the cleared ones resulted in a positive profit.

Alias ID 1, which is the most *active* market participant in terms of the number of submitted CBs, used the Opportunistic Strategy in *most* of the nodes. Fig. 2.8 shows the hourly per unit profit for Alias ID 1 at four different locations using the Opportunistic Strategy. It should be mentioned that only the non-zero profits are shown in Fig. 2.8. As we can see, there are only a few days that *any* of the submitted CBs is cleared. But Alias ID 1 had excellent profit on those few days. For these CBs, CSR and LPR are 0.24% and 3.04%, respectively. These values show that only a few submitted CBs are cleared, but most of the cleared ones resulted in a positive profit.

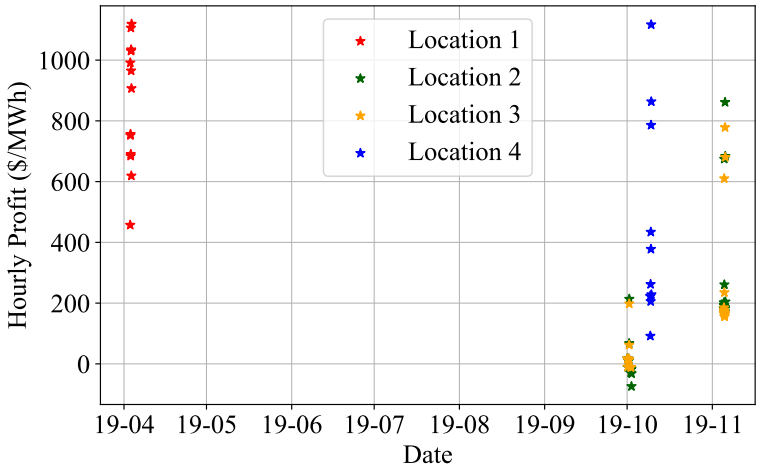

Figure 2.8: Hourly profit for Alias ID 1 using the Opportunistic Strategy at four different locations in the market.

Alias ID 11 always used the Self-Scheduling Strategy as its strategy. As mentioned in Section 2.3.2, this strategy is *less* common among the market participants. Fig. 2.6 shows that Alias ID 11 did *not* gain a high profit during its presence in the market despite participating in more than 300 nodes. From Table 2.3, almost 100% of Alias ID 11's CBs are cleared in the market. For this market participant, CSR is 90.90%.

The share of each implemented CB strategy for each CB market participant is calculated. The results for each of the 20 most present CB market participants are shown in Fig. 10. This figure shows the share of each strategy for each Alias ID. We can see that each of the three identified convergence bidding strategies has been used in the market.

In total, out of the 6.6 million submitted CBs that were analyzed during the period of this study for all the 101 CB market participants in the California ISO market, here is the share of each convergence bidding strategy: 35.95% of all the submitted CBs belong to CB Cluster 1 (Price-Forecasting Strategy), 15.58% of all the submitted CBs belong to

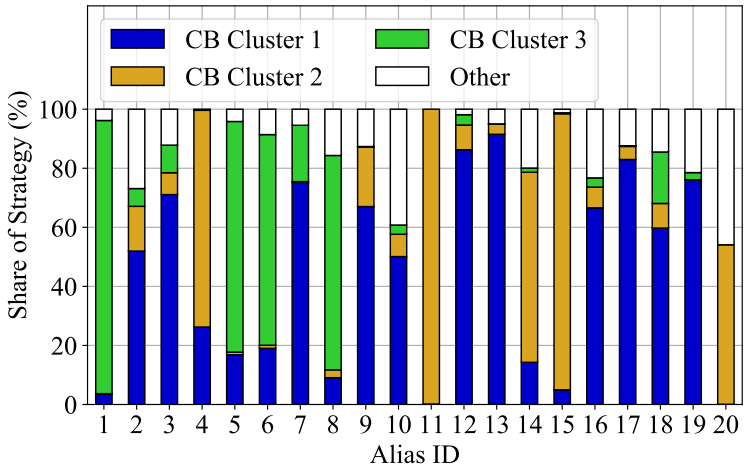

Figure 2.9: The share of each identified strategy for each market participant.

CB Cluster 2 (Self-Scheduling Strategy), 35.33% belong to CB Cluster 3 (Opportunistic Strategy), and 13.14% of all the submitted CBs belong to Other (Unidentified) strategies.

As it is evident from the above numbers, *three* is the exact number of the clusters of strategies that take *significant shares* of the real-world convergence bids in the period of this study. On one hand, a smaller number of clusters would inevitably ignore at least one of the three significant real-world strategies. On the other hand, a larger number would inevitably add a very insignificant strategy which can distract the focus from the three significant strategies and their characteristics and implications.

Collectively, the analyses in Sections 2.3.2 and 2.3.3 address Research Question 4 that we had raised in Section 1.4.

2.4 Designing a Comprehensive Convergence Bidding Strategy Based on the Reverse Engineering Results

In this section, we seek to address Research Question 5. In this regard, we propose a new comprehensive composite convergence bidding strategy based on the results in Section 2.3. The key question is: *now that we have learned the strategic behaviors of various real-world CB market participants through reverse engineering, can we go one step further and create a new CB strategy that can learn from the advantages and disadvantages of the existing strategies to significantly outperform them?* The answer is *yes*. In this section, we discuss how such a strategy can be developed.

The proposed composite convergence bidding strategy is developed in three steps. ***First***, we focus on the Opportunistic Strategy, i.e., the CB strategy that is completely new and has never been discussed in the literature. In this step, we propose an optimization-based algorithm to maximize the net profit of the market participant by *capturing the spikes* in D-LMPs with an optimal price bid at each node. ***Second***, we introduce an algorithm to *label* each node based on the solution of the optimization problem in the first step. This labeling is necessary to find out what kind of CB (if any) is more profitable at each node. Each node can be labeled as Demand CB Node, or Supply CB Node, or Neither, or Both. ***Third***, by using the results from the first two steps, and combining them with the results from Section 2.3 about CB Cluster 1 and CB Cluster 2, we propose the new composite CB strategy.

2.4.1 Step 1: Net Profit Maximization by Capturing Price Spikes

Basic Idea

We define *price spikes* as the cases where D-LMPs demonstrate abnormalities by being much higher or much lower than the average D-LMP at the same location and the same hour. By using the historical data at each node, we formulate an optimization problem to find the *optimal price bid* that could maximize the net profit with *minimum loss* for a CB with a unit quantity. If there is a feasible solution for the formulated optimization problem, then the optimal price bid will be used for each hour of the next day for that given node. Price spikes can be both negative or positive. A demand CB is required to take advantage of a negative spike in D-LMPs, i.e., low prices. Similarly, a supply CB is required to take advantage of a positive spike in D-LMPs, i.e., high prices.

Optimization Problem Formulations

The following optimization problem is designed to capture the negative spikes with a demand CB at each node in order to maximize the total net profit with minimum loss. At each time interval, if the net profit (η_t) is positive, then it is considered as a profit (P_t); and if it is negative, then it is considered as a loss (L_t). Note that, this optimization problem makes use of only the historical data that are already known to the market participant. Thus, it does *not* require dealing with the difficulties associated with price forecasting. Hence, this analysis is inherently not sensitive to the accuracy of price forecasting. Here, T is the set of historical time intervals that a market participant considers in analyzing the historical price spikes.

$$\text{maximize} \qquad Obj : \sum_{t=1}^{T} \eta_t \tag{2.3}$$

$$\text{subject to} \qquad \eta_t = (\pi_t - \lambda_t) \mid \lambda_t \leq x_t, \qquad \forall t \in T \tag{2.4}$$

$$x_t = \lambda_t^* - m \qquad \forall t \in T \tag{2.5}$$

$$P_t = \eta_t \mid \eta_t \geq 0, \qquad \forall t \in T \tag{2.6}$$

$$L_t = \eta_t \mid \eta_t \leq 0, \qquad \forall t \in T \tag{2.7}$$

$$-\sum_{t=1}^{T} L_t \leq \epsilon \times \sum_{t=1}^{T} P_t \tag{2.8}$$

$$m^{min} \leq m \leq m^{max} \tag{2.9}$$

The objective function (2.3) is the total net profit over the past T time intervals. The amount of net profit for each time interval using a demand CB with a unit quantity is calculated in (2.4). Here, π and λ denote R-LMP and D-LMP, respectively; and x is the price bid. The *condition* in this constraint, which is denoted by a vertical line, indicates that the submitted price bid (x) is cleared *only if* it is higher than D-LMP. Eq. (2.5) shows that the price bid for each hour is equal to the average of D-LMP for that hour minus m. In this optimization, m is the main decision variable which is the *distance* from the average hourly D-LMPs that is captured as a *price spike criteria* by an optimal price bid. Eqs. (2.6) and (2.7) divide the net profit to *profit* and *loss* in each time interval. Eq. (2.8) is a bound constraint that is used to guarantee that the total amount of loss is less than a small percentage (ϵ) of the total amount of profit. As we will discuss in Step 2 of the proposed method, only those nodes that have a *feasible solution* for this optimization problem with

an optimal objective value of greater than a *threshold* are used in our proposed bidding strategy.

As mentioned before, the optimization problem in (2.3)-(2.9) is for capturing the *negative* spikes in D-LMPs with demand CBs. The same optimization problem can be used to capture the *positive* spikes with supply CBs. We just need to replace the definition of net profit in (2.4)-(2.5) with the following:

$$\eta_t = (\lambda_t - \pi_t) \mid \lambda_t \geq x_t, \qquad \forall t \in T \tag{2.10}$$

$$x_t = \lambda_t^* + m \qquad \forall t \in T \tag{2.11}$$

Solving the Formulated Problems

The introduced optimization problems are *non-convex* and may not be solved efficiently and quickly in their current forms. Importantly, it is necessary to have a computationally tractable formulation as these optimization problems must be solved *each* day for *all* the nodes in the market. In two steps, we convert the optimization problem (2.3)-(2.9) into a Mixed-Integer Linear Program (MILP). First, we introduce a binary variable (b_t^1) and utilize the Big-M method to convert Eq. (2.4) to the following linear constraints [46]:

$$\eta_t = b_t^1 \times (\pi_t - \lambda_t), \qquad \forall t \in T \tag{2.12}$$

$$x \geq \lambda_t - M \times (1 - b_t^1), \qquad \forall t \in T \tag{2.13}$$

$$x \leq \lambda_t + M \times b_t^1, \qquad \forall t \in T \tag{2.14}$$

where M is a large fixed parameter in the Big-M method. Next, equations (2.6)-(2.7) are transformed to the following:

$$P_t = \eta_t \times b_t^2 \qquad \forall t \in T \tag{2.15}$$

$$L_t = \eta_t \times (1 - b_t^2), \qquad \forall t \in T \tag{2.16}$$

$$\eta_t \geq -M \times (1 - b_t^2), \qquad \forall t \in T \tag{2.17}$$

$$\eta_t \leq M \times b_t^2, \qquad \forall t \in T \tag{2.18}$$

where b^1 and b^2 are binary variables. By replacing R_t in equations (2.15)-(2.18) with equation (2.12), the new MILP maximization problem will be formulated as follows:

$$\text{maximize} \qquad Obj : \sum_{t=1}^{T} b_t^1 \times (\pi_t - \lambda_t) \tag{2.19}$$

$$\text{subject to} \qquad \lambda_t^* - m \geq \lambda_t - M(1 - b_t^1), \qquad \forall t \in T \tag{2.20}$$

$$\lambda_t^* - m \leq \lambda_t + M \times b_t^1, \qquad \forall t \in T \tag{2.21}$$

$$b_t^1 \times (\pi_t - \lambda_t) \geq -M(1 - b_t^2), \qquad \forall t \in T \tag{2.22}$$

$$b_t^1 \times (\pi_t - \lambda_t) \leq M \times b_t^2, \qquad \forall t \in T \tag{2.23}$$

$$\sum_{t=1}^{T} (z_t - b_t^1) \times (\pi_t - \lambda_t) \leq \epsilon \times \sum_{t=1}^{T} z_t \times (\pi_t - \lambda_t) \tag{2.24}$$

$$m^{min} \leq m \leq m^{max} \tag{2.25}$$

$$z_t \leq b_t^1, \qquad \forall t \in T \tag{2.26}$$

$$z_t \leq b_t^2, \qquad \forall t \in T \tag{2.27}$$

$$z_t \geq b_t^1 + b_t^2 - 1, \qquad \forall t \in T \tag{2.28}$$

$$0 \leq z_t \leq 1, \qquad \forall t \in T \tag{2.29}$$

The optimization problem in (2.19)-(2.29) is the linearized version of the optimization problem in (2.3)-(2.9). The process of linearizing this optimization problem is done through (2.12)-(2.18). Note that, z is a *new* continuous auxiliary variable which takes the value of the multiplication of b^1 and b^2 to avoid the nonlinearity. Constraints (2.26)-(2.29) are added to the linearized optimization problem in order to create the required conditions for z to be able to work as the multiplication of b^1 and b^2. This final MILP optimization problem in (2.19)-(2.29) can be solved by using various commercial solvers.

2.4.2 Step 2: Dynamic Node Labeling

Algorithm 1 is developed to dynamically *label* each node for the next day, using the optimization-based results in Step 1. For each node, first, we solve the negative and the positive spike capturing problems. If the *optimal objective value* for the negative spike capturing problem is greater than a threshold, then the node is labeled as Demand CB Node. If the *optimal objective value* for the positive spike capturing problem is greater than a threshold, then the node is labeled as Supply CB Node. The two optimization problems are independent; hence, a node can be labeled *both* as Demand CB Node and Supply CB Node. A node may also be labeled as No CB Node.

As another output of the optimization problem in (2.19)-(2.29), m is used for generating the optimal price bid for each hour of the next day based on the label of each node. If a node is labeled as Demand CB Node, Supply CB Node, or Both, then it will be considered for the next (final) step in the proposed convergence bidding strategy, as we will explain next.

Algorithm 1 Dynamic Node Labeling

Input: Outputs of Optimization-Based Spike Capturing

Output: Label and Optimal Price Bid for each Node

for n in Nodes **do**

    Solve the negative spike capturing problem in (2.3)-(2.9).

    if $Obj > \theta$ **then**

        Label n as a *Demand CB Node*

        Optimal Price Bid $= \lambda_t^* - m$

    end if

    Solve the positive spike capturing problem in (2.3), (2.6)-(2.11).

    if $Obj > \theta$ **then**

        Label n as a *Supply CB Node*

        Optimal Price Bid $= \lambda_t^* + m$

    end if

end for

2.4.3 Step 3: Strategy Selection

In this section, we put together all the components, including the optimization-based price spike capturing method in Step 1 and the dynamic node labeling method in Step 2 to develop a new composite convergence bidding strategy. The new CB strategy makes use of each of three reverse engineering CB strategies based on their advantages and disadvantages.

The inputs for this comprehensive strategy are the historical LMPs and the forecasted LMPs for the next day. The output is the type of strategy that should be used at each node for each hour of the next day. The outline of this strategy is shown in Fig. 2.10. Here, a^{λ}, a^{π}, and a^{δ} are the accuracy for the forecasted D-LMP, R-LMP, and the sign of the difference between D-LMP and R-LMP, respectively. As we can see, the first two strategies in this algorithm are based on the *forecast accuracy* of the next day LMPs. On the other hand, the third strategy does not use any price forecast data and instead, relies on the historical LMPs, optimization-based price spike capturing, and node labeling. It must be mentioned that these three strategies are based on the three identified clusters of strategies in Section 2.3.2. The choice of the thresholds for the mentioned forecast accuracy defines the risk preference for the use of each strategy. Higher thresholds in Fig. 2.10, mean less risk-seeking; and lower thresholds mean more risk-seeking. The application of each strategy is as follows:

Selecting CB Strategy 1: This strategy is selected if both D-LMP and R-LMP forecasts are available and have high accuracy. For each hour of the next day, if the forecasted D-LMP is higher than R-LMP, then a supply CB is submitted. If the forecasted R-LMP is higher than D-LMP, then a demand CB is submitted. For a supply CB, the price components should be *less* than the forecasted D-LMP but *close* to it in order to avoid entering the market when D-LMP is unexpectedly low. Also, for a demand CB, the price components should be *more* than the forecasted D-LMP but *close* to it in order to avoid entering the market when D-LMP is unexpectedly high.

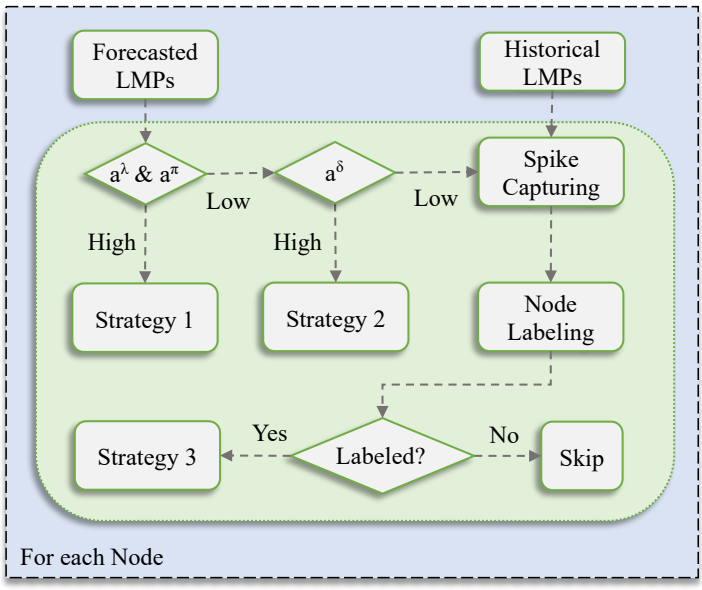

Figure 2.10: The proposed comprehensive convergence bidding strategy for each hour of the next day and at each node in the market, based on the reversed engineered strategies of market participants.

Selecting CB Strategy 2: This strategy should be used if only the forecast for the sign of the difference between D-LMP and R-LMP is available and it has high accuracy. For each hour of the next day, if the difference between D-LMP and R-LMP is *positive*, then a supply CB is submitted; and if it is *negative*, then a demand CB is submitted. The price components for a supply CB must be *much lower* than the average D-LMP; and for a demand CB, it must be *much higher* than the average D-LMP on that hour in order to always be cleared in the market.

Selecting CB Strategy 3: This strategy is used when accurate forecasting for LMPs are *not* available at a node. Using the historical LMPs in the spike capturing optimization problem and the node labeling algorithm, the optimal price bid and the type of CB are determined for a node. As explained in Step 1, the optimal price component of the

submitted CB is the best price bid to capture the price spikes; which leads to a situation where the convergence bidders participate in the CB market only occasionally, but when their CB is cleared they gain considerable profit. This behavior is indeed justified, because in the absence of accurate price forecasting capability, one should avoid taking high risks.

It must be emphasized that, each strategy has its own importance and it forms part of the proposed enhanced composite bidding strategy. For example, although we showed that the performance of the Self-Scheduling Strategy is not as good as the other two strategies in the California ISO market, the Self-Scheduling Strategy does bring value to our composite bidding strategy when there is an accurate forecast only for the sign of the difference between D-LMP and R-LMP. If there is an accurate forecast for both D-LMP and R-LMP, then the Price-Forecasting Strategy would be a better choice.

Importantly, the construction of the above proposed algorithm also addresses Research Question 6. Here, the seemingly unprofitable (or low profitable) CB strategy is the second strategy. It is now incorporated as one part of an enhanced and profitable new bidding strategy.

Another note to mention is that, the overall architecture of our proposed composite bidding strategy is *not* sensitive to or even directly related to the specific building of the explained clusters. That is, if other major clusters of bidding strategies emerge in the future, they too can potentially be incorporated into the architecture of our proposed composite bidding strategy by reveres engineering their main characteristics.

Before ending this section, it should be mentioned that the quantity of submitted CBs (MWh) at each hour, depends on the available credit for each market participant with

the California ISO. Accordingly, a unit value is considered in the proposed bidding strategy for the quantity of submitted CBs, which is aligned with other studies in the literature such as [34].

2.4.4 Case Study

In this section, we analyze the performance of the proposed comprehensive convergence bidding strategy. Since providing an accurate and realistic forecast for D-LMPs and R-LMPs is out of the scope of this work, here we assume that we have the same forecasting accuracy as Alias ID 9, which is the most lucrative CB market participant in the California ISO market during the period of this study. Our goal here is to examine how Alias ID 9 could improve its performance in 2019, if it had used our proposed composite strategy. The value for M in the Big-M method is tuned to be a sufficiently large number. In this regard, it is set to 3000. Also, the boundaries for m in equation (2.25) are set to 30 and 200, respectively; which are based on our observations on the real-world data. The analyses in this section are done in Python and the optimization problems are solved by using Gurobi within the Pyomo package on a PC with Intel Xeon Silver 4208 CPU @2.10GHz and 128 GB RAM.

As mentioned before, Alias ID 9 mostly participated in the main Hubs and DLAPs by utilizing the Price-Forecasting Strategy. For other nodes, we use one year of historical data before each day in 2019 and run the dynamic node labeling algorithm including the optimization-based spike capturing problem. By adjusting the only two hyperparameters, ϵ and θ, the nodes with the potential to use the Opportunistic Strategy are labeled and the optimal price bid is submitted for each hour of the next day. The submitted CBs have one

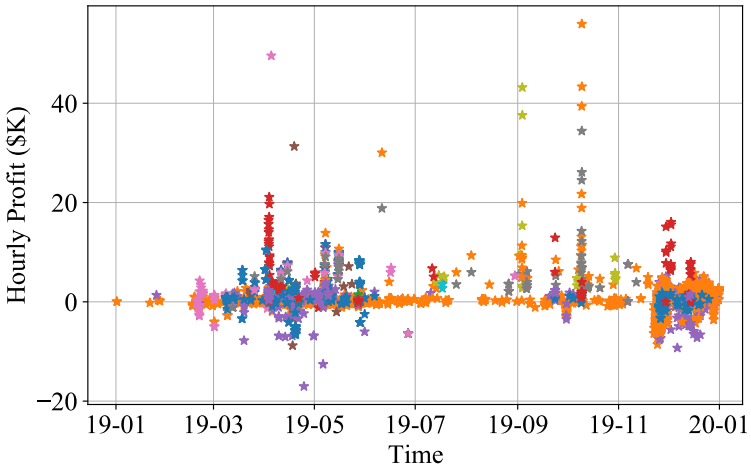

Figure 2.11: The *additional* hourly net profit in Case 1. Each color represents one of the 148 labeled nodes where the submitted CBs are cleared.

step and the quantity of each submitted CB is considered as the average of Alias ID 9's submitted CBs equal to 50 MW, instead of a unit value. All the above assumptions match the overview of the actual market data in Table 2.2.

Table 2.4 shows three cases based on different values for the hyperparameters. We can see that, by tightening the constraints (decreasing ϵ and increasing θ) from Case 1 to Case 3, the number of nodes and days that the submitted CBs are cleared has decreased. As we defined in (2.2), LPR indicates the level of loss compared to the level of profit. Also, recall from Section 2.4.1 that η denotes the total net profit. As we can see in Table 2.4, by tightening the constraints, although the total net profit is decreased, the loss-to-profit-ratio as an important factor in the Opportunistic Strategy is also decreased. Therefore, these two parameters can be used as control knobs by the market participant to suitably adjust the level of risk seeking in this composite bidding strategy. Figs. 2.11 and 2.12 show the

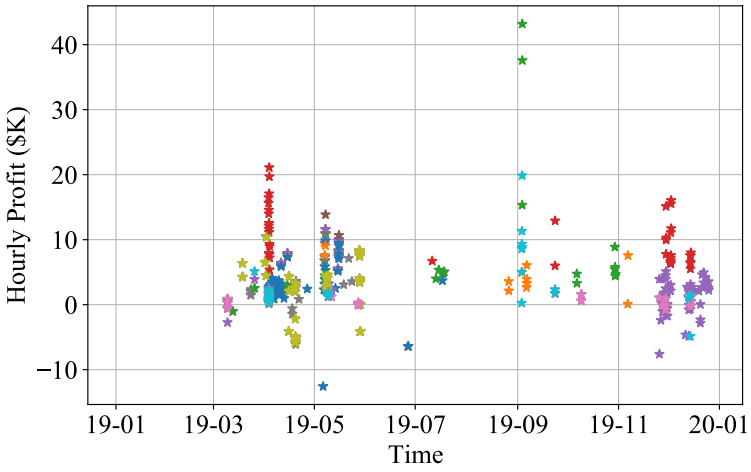

Figure 2.12: The *additional* hourly net profit in Case 2. Each color represents one of the 32 labeled nodes where the submitted CBs are cleared.

additional hourly net profit for Case 1 and Case 2. Note that, notation \$K means \$1,000. In Fig. 2.12, for Case 2 as a moderate case, it is shown that by submitting CBs at 32 nodes and entering the CB market in only 66 days, Alias ID 9 could earn an *additional* net profit of \$2.13 million. This is a 43% increase in Alias ID 9's net profit in 2019, compared to its current net profit of \$4.9 million. In order to further extended the assessment of the increase in net profit, Table 2.5 shows the original annual net profit of four market participants (Alias IDs) in 2019 and compares them with the corresponding annual net profit of the same market participant in case she had used the proposed convergence bidding method in Algorithm 1. Similar to the previous test case for Alias ID 9 as the most lucrative market participant, here we use the average quantity in MWh from Table 2.2 for the size of the CBs for each market participant. We can see that all these four market participants that were mainly focused on the third strategy based on Fig. 10, could have significantly benefited from the proposed convergence bidding strategy.

2.5 Conclusions

This chapter provided a data-driven analysis of real-world electricity market data from the California ISO market to *understand*, *reverse engineer*, and *enhance* the behavior of convergence bidders. It was discussed that a total of 20 CB market participants currently have a considerable presence in the California ISO that accounts for 72% to 84% of the entire CB market. The different bidding characteristics of these most present market participants were analyzed. Next, four quantitative features were extracted from all the submitted CBs; and by using the HDBSCAN algorithm, three main clusters of CB strategies were identified. The characteristics and the performance of each identified cluster of strategies were analyzed and some of their *advantages* and *disadvantages* were investigated.

Two interesting discoveries were discussed. First, the Opportunistic Strategy does *not* match any of the convergence bidding strategies that currently exist in the literature. Second, most papers in the literature are focused on the Self-Scheduling Strategy, while in practice, this strategy is *less* common among the market participants in the California ISO.

After reverse engineering the convergence bidding strategies of the real-world market participants in the California ISO market, a new comprehensive *composite* CB strategy was proposed. It was shown that the proposed strategy, optimally utilizes the advantages of various identified reverse engineered strategies under different market conditions. The new strategy was developed in three steps: First, by focusing on the Opportunistic Strategy as the newly discovered strategy, an optimization-based algorithm was proposed to maximize the total net profit of the market participant by capturing the price spikes. Second, an algorithm was developed to dynamically label each node based on the solution of the

optimization problem in the first step. Third, by using the results from the first two steps for the Opportunistic Strategy, as well as by combining them with the Price-Forecasting Strategy and the Self-Scheduling Strategy, a strategy selection algorithm was proposed to complete a comprehensive composite CB strategy. It was shown in a case study that the annual profit of the most lucrative market participant could increase by over 40% if the proposed comprehensive strategy had been used.

Table 2.1: Selection of the CB Market Participants with Considerable Presence based on the Four Introduced Metrics across a Total of 101 Convergence Bidders.

Alias ID	①	②	③	④
1	20.97	1.49	11.06	1.93
2	8.53	12.82	5.61	7.00
3	6.54	8.92	1.68	2.51
4	6.05	13.13	3.00	6.96
5	6.02	1.26	16.26	3.47
6	5.63	1.50	7.09	3.55
7	5.26	1.16	2.28	0.50
8	3.87	1.11	2.34	1.21
9	3.69	7.15	10.56	17.56
10	2.56	3.30	0.68	1.06
11	2.49	5.62	0.31	0.72
12	2.31	2.92	1.11	1.47
13	1.91	2.24	5.77	5.82
14	1.67	3.63	0.28	0.62
15	1.58	3.53	0.27	0.62
16	1.36	2.37	1.76	2.10
17	1.21	1.90	4.58	5.10
18	1.11	1.12	2.20	2.71
19	1.04	1.94	2.50	3.69
20	0.19	0.41	1.88	4.30
Total	84.0%	77.5%	81.2%	72.9%

① Share of the number of submitted CBs (%).

② Share of the number of cleared CBs (%).

③ Share of the total submitted quantity in MWh (%).

④ Share of the total cleared quantity in MWh (%).

Table 2.2: Convergence Bidding Characteristics in the Cleared CBs for the Market Participants with Considerable Presence.

Alias ID	①	②	③	④
1	28.21	68.11	2.86	28.79
2	58.53	79.08	1.11	8.41
3	70.95	69.33	2.05	4.92
4	95.37	50.53	1	7.97
5	21.47	63.18	2.9	76.51
6	48.63	57.01	1.92	49.27
7	62.11	61.5	2.45	8.07
8	19.16	49.12	1.64	19.73
9	18.11	55.08	2.52	49.66
10	32.63	79.03	1.04	4.97
11	68.63	45.74	1	1.92
12	20	58.02	1.03	7.84
13	3.58	53.81	1.37	49.15
14	24.84	60.19	1.13	2.6
15	45.26	39.25	1	2.64
16	22.74	77.88	4.36	21.42
17	12	87.04	3.33	53.93
18	33.68	53.63	1	36.23
19	69.89	64.09	5.29	37.37
20	0.21	100	1	156.72

① Share of nodal locations in cleared CBs (%).

② Share of supply bids in cleared CBs (%).

③ Average number of steps in cleared CBs.

④ Average quantity in MWh in cleared CBs.

Table 2.3: Percentage of Submitted CBs that Are Cleared in the Market for Each Alias ID in Each Year.

Alias ID	2017 (%)	2018 (%)	2019 (%)
1	3.58	3.59	2.45
2	66.12	65.72	67.36
3	68.43	68.86	48.32
4	-	98.68	94.38
5	33.46	12.54	5.25
6	7.29	14.41	44.49
7	5.52	13.48	11.51
8	100	4.54	14.23
9	88.36	94.15	76.77
10	56.99	60.57	40.17
11	-	99.84	99.98
12	-	61.14	54.99
13	61.14	51.78	51.12
14	98.19	93.11	95.54
15	96.45	99.9	99.79
16	68.81	81	75.64
17	86.43	88.15	49.98
18	82	59.73	33.62
19	78.45	83.99	84.15
20	98.79	98.13	-

Table 2.4: Results for Three Analyzed Cases Based on Different Values of the Hyperparameters.

Case	ϵ	θ	Node	Day	η ($M)	LPR (%)
1	0.01	100	148	227	3.89	24.84
2	0.001	1000	32	66	2.13	11.14
3	0.0001	2000	25	40	1.55	5.25

Table 2.5: Comparing the Performance of the Proposed Method with Four Alias ID in 2019 which Mostly Used the Third Strategy.

Alias ID	Original Net Profit ($M)	New Net Profit ($M)	Improvement ($M)
1	0.30	1.27	0.97
5	0.31	3.26	2.95
6	0.44	2.1	1.66
8	0.58	0.84	0.26

Chapter 3

Understanding Convergence Bids During Blackouts: Analytical Results and Real-World Implications

3.1 Introduction

In this chapter, we investigate the operation and impact of CBs during *blackouts*. First, the amount of load shedding in the RTM is modeled as a function of the amount of the cleared CBs in the DAM. The sign of the slope of this function is proposed as a metric to determine if a CB *exacerbates* or *heals* the power outages. Next, a series of mathematical theorems are developed to obtain and characterize this new metric under different network

conditions. It is proved that, when there is *no* congestion in the DAM, the metric is always greater than or equal to zero. When there *is* congestion in the DAM, the metric can be positive or negative. Using numerical case studies, we show that, not only when there is no congestion, but also most often when there is congestion, the introduced metric is positive. Therefore, supply CBs almost always hurt the system during blackouts while demand CBs almost always help the system. Furthermore, the impact of load shedding on the profit of CBs is also analyzed. It is shown that, load shedding usually creates advantage for supply CBs and disadvantage for demand CBs in terms of their profit. This might be unfair; because as we mentioned, supply CBs exacerbate the power outages while demand CBs heal the outages. The implications of these results are discussed. We also analyze the real-world market data from the California Independent System Operator (ISO) during the blackouts in August 2020 to better understand the implications of the above results. It is shown that, the decision by the California ISO to suspend CBs during this event does very well matches the mathematical and numerical results that are obtained and discussed in this chapter.

3.1.1 Summary of Contributions and Discoveries

The discoveries and contributions in this chapter are as follow:

- Obtaining rigorous analytical formulations to capture and explain the relationship between load shedding and convergence bidding during power outages. To the best of our knowledge, this is the first work to study the operation and impact of CBs during power outages.

- The amount of load shedding in the RTM is modeled as a *function* of the amount of the cleared CBs in the DAM. The sign of the slope of this function is examined as a new metric to determine if a cleared CB is *exacerbating* or *healing* the power outages. We mathematically obtain this metric under different network conditions.

- It is proved that, when there is *no* congestion in the DAM, the metric is always greater than or equal to zero. When there *is* congestion in the DAM, the metric can be positive or negative. We explain how this can happen based on the parameters of the system. These results clearly show that, despite being financial instruments in the DAM, CBs can affect load shedding in the RTM.

- We use numerical case studies to confirm the analytical results. Importantly, we show that, not only when there is no congestion, but most often even when there is congestion, the new metric is positive. The conditions for the metric to be negative is very rare. Therefore, we conclude that supply (demand) CBs almost always hurt (help) the system during major power outages.

- Furthermore, we also examine how load shedding can affect the profit of CBs. Our analysis in this part is again both analytical and numerical. We show that load shedding usually creates advantage for supply CBs and disadvantage for demand CBs in terms of their profit in the electricity market. This might be unfair; because as we previously mentioned, supply CBs exacerbate the power outages while demand CBs heal the outages.

- The real-world market data from the California ISO during the blackouts in August 2020 are analyzed to better understand the implications of the above results. By analyzing the market data, we show that the decision by the California ISO to suspend CBs during expected outage conditions very well matches the mathematical and numerical results that we obtained in this study.

3.2 Relationship between Convergence Bidding and Load Shedding

In order to understand the potential impact of CBs during blackouts, we need to obtain the relationship between the cleared CBs in the DAM and the amount of load shedding in the RTM. This can be done mathematically by expressing load shedding as a *function* of the cleared CBs; as we will discuss in details throughout this section.

3.2.1 Basic Market Formulations

Understanding the role of CBs in electricity markets requires examining both the DAM and the RTM.

First, consider the following DAM optimization problem:

$$\underset{\mathbf{x},\mathbf{z}}{\text{minimize}} \qquad 0.5\,\mathbf{x}^T\mathbf{A}\,\mathbf{x} + \mathbf{b}^T\mathbf{x} - (0.5\,\mathbf{z}^T\mathbf{C}\,\mathbf{z} + \mathbf{d}^T\mathbf{z}) \tag{3.1}$$

$$\text{subject to} \qquad \mathbf{1}^T\mathbf{x} - \mathbf{1}^T\mathbf{z} + \mathbf{1}^T\mathbf{v} = 0 \tag{3.2}$$

$$-\mathbf{c} \leq \mathbf{S}(\mathbf{\Psi}\,\mathbf{x} - \mathbf{\Theta}\,\mathbf{z} + \mathbf{\Omega}\,\mathbf{v}) \leq \mathbf{c} \tag{3.3}$$

$$\mathbf{x}^{\min} \leq \mathbf{x} \leq \mathbf{x}^{\max} \tag{3.4}$$

$$\mathbf{z}^{\min} \leq \mathbf{z} \leq \mathbf{z}^{\max} \tag{3.5}$$

where $\mathbf{x}$ is the vector of generation bids; $\mathbf{z}$ is the vector of demand bids; and $\mathbf{v}$ is the vector of CBs. Matrix $\mathbf{S}$ contains the shift factors in the network; and $\mathbf{c}$ is the vector of transmission line capacities. Matrices $\mathbf{\Psi}$, $\mathbf{\Theta}$, and $\mathbf{\Omega}$ are the incidence matrices for generation bids, demand bids, and CBs, respectively. Matrices $\mathbf{A}$ and $\mathbf{C}$ and vectors $\mathbf{b}$ and $\mathbf{d}$ are the quadratic linear coefficients for the generation and demand bids, respectively. The basic market formulation in (3.1)-(3.5) is commonly used in the literature, c.f. [4, 12, 40, 47].

Once the DAM is cleared, we can obtain the total amount of the cleared CBs in the DAM as follows:

$$CB = \mathbf{1}^T \mathbf{v}^*, \tag{3.6}$$

where $\mathbf{v}^*$ is the optimal solution in (3.1)-(3.5) for the CBs.

Next, consider the following RTM optimization problem:

$$\underset{\mathbf{y}}{\text{minimize}} \qquad 0.5\, \mathbf{y}^T \mathbf{E}\, \mathbf{y} + \mathbf{k}^T \mathbf{y} \tag{3.7}$$

$$\text{subject to} \qquad \mathbf{1}^T \mathbf{y} - \mathbf{1}^T \mathbf{L} = 0 \tag{3.8}$$

$$-\mathbf{c} \leq \mathbf{S}(\mathbf{\Psi}\, \mathbf{y} - \mathbf{\Theta}\, \mathbf{L}) \leq \mathbf{c} \tag{3.9}$$

$$\mathbf{x}^{\min} \leq \mathbf{y} \leq \mathbf{x}^{\max} \tag{3.10}$$

$$\mathbf{g}(\mathbf{x}^*) \leq \mathbf{y} \leq \mathbf{h}(\mathbf{x}^*) \tag{3.11}$$

where $\mathbf{y}$ is the vector of the *actual* generation in the RTM; and $\mathbf{L}$ is the vector of the *actual* consumption in the RTM. Parameters $\mathbf{c}$, $\mathbf{x}^{\min}$, and $\mathbf{x}^{\max}$ are the same as in the DAM

problem. Matrix $\mathbf{E}$ and vector $\mathbf{k}$ are the quadratic and linear coefficients of the generation bids in the RTM, respectively.

Regarding notations $\mathbf{g}(\cdot)$ and $\mathbf{h}(\cdot)$ in the constraint in (3.11), they limit the actual output of the generation units in the RTM based on the outcome of the DAM optimization problem in (3.1)-(3.5). Here, $\mathbf{x}^*$ is the optimal generation schedule in the DAM optimization problem. Functions $\mathbf{g}(\cdot)$ and $\mathbf{h}(\cdot)$ is set for each generator based on its operational requirements [48]. For example, some generators cannot lower their actual output below their optimal DAM schedule. As a special case, one can set $\mathbf{g}(\mathbf{x}^*) = \mathbf{x}^*$ and $\mathbf{h}(\mathbf{x}^*) = \mathbf{x}^{\max}$, which in that case, the formulation in (3.7)-(3.11) matches the one in [4]. However, our analysis in this study is general; and we do not need to choose any specific form of functions for $\mathbf{h}(\cdot)$ and $\mathbf{g}(\cdot)$. Our only assumption is that, for each generator i, we have $g_i(\cdot) < h_i(\cdot)$, i.e., the lower bound cannot exceed the upper bound; and function $h_i(\cdot)$ is non-decreasing, i.e., a higher generation schedule in the DAM may not cause a lower upper bound for the actual generation in the RTM.

3.2.2 Analysis of Load Shedding

Once the power grid exceeds its generation capacity or its transmission capacity, load shedding becomes necessary in order to maintain a stable operation. The concept of load shedding is inherently relevant *only* to the real-time operation of the system in the RTM. It is *not* relevant to in the DAM.

In order to analyze the RTM under the circumstances of load shedding, we must examine the *Feasibility Check Subproblem* (FCSP) in the RTM. If the RTM optimization problem in (3.7)-(3.11) is infeasible, then it requires load shedding. Of main concern here

is the *minimum* amount of load shedding that is required in order to make the RTM optimization feasible:

$$\underset{\mathbf{s},\mathbf{y}}{\text{minimize}} \quad \mathbf{1}^T\mathbf{s} \tag{3.12}$$

$$\text{subject to} \quad \mathbf{1}^T\mathbf{y} - \mathbf{1}^T(\mathbf{L} - \mathbf{s}) = 0 \tag{3.13}$$

$$-\mathbf{c} \leq \mathbf{S}(\mathbf{\Psi}\,\mathbf{y} - \mathbf{\Theta}\,(\mathbf{L} - \mathbf{s})) \leq \mathbf{c} \tag{3.14}$$

$$\mathbf{x}^{\min} \leq \mathbf{y} \leq \mathbf{x}^{\max} \tag{3.15}$$

$$\mathbf{g}(\mathbf{x}^*) \leq \mathbf{y} \leq \mathbf{h}(\mathbf{x}^*) \tag{3.16}$$

$$\mathbf{s} \geq \mathbf{0} \tag{3.17}$$

where $\mathbf{s}$ is the vector of minimum required load shedding. The rest of the notations in (3.12)-(3.17) are the same as those in the basic RTM optimization problem in (3.7)-(3.11).

Once the FCSP is solved, we are interested in examining the total amount of load shedding in the system:

$$LS = \mathbf{1}^T\mathbf{s}^*, \tag{3.18}$$

where $\mathbf{s}^*$ is the optimal solution of the FCSP in (3.12)-(3.17).

3.2.3 Impact of Convergence Bids on Load Shedding

Let us define the following *functional* relationship between the amount of the cleared CBs in the DAM and the total amount of load shedding per the FCSP in the RTM:

$$LS = f(CB), \tag{3.19}$$

where CB is defined in (3.6) and LS is defined in (3.18).

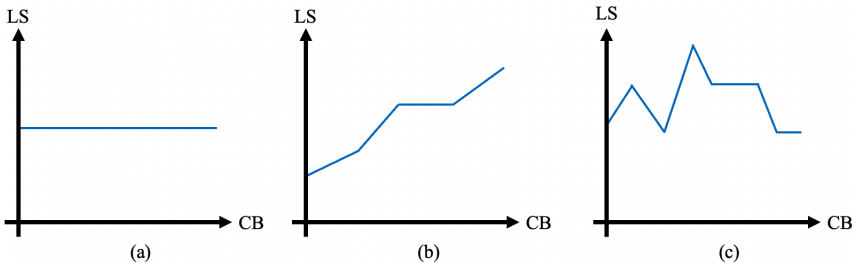

Figure 3.1: Three cases for load shedding as a function of cleared CBs: (a) No Impact; (b) Monotone Impact; (c) Non-Monotone Impact.

Consider the *slope* of the above functional relationship:

$$\frac{\Delta LS}{\Delta CB}. \tag{3.20}$$

If the *slope* is positive, then an increase in the amount of the cleared CBs results in *more* load shedding in the system. If the *slope* is negative, then an increase in the amount of the cleared CBs results in *less* load shedding in the system.

In this regard, we can distinguish three cases with respect to the impact of cleared CBs on the amount of load shedding:

Case 1 (No Impact): There is no relation between the total amount of load shedding and the amount of the cleared CBs. Accordingly, the *slope* in (3.20) is always zero, and function $f(\cdot)$ is always *flat*, see Fig. 2(a). Interestingly, this case matches the implicit assumption in the existing literature about CBs. Since CBs are financial instruments in the DAM, while load shedding is a physical action in the RTM, it is generally assumed that CBs do *not* have any impact on load shedding.

Case 2 (Monotone Impact): There is a direct and monotone relationship between the total amount of load shedding and the amount of the cleared CBs. If the relationship is monotone increasing, then the *slope* in (3.20) is always positive. If the relationship is

monotone decreasing, then the *slope* in (3.20) is always negative. An example for a monotone relationship is shown in Fig. 2(b), where the *slope* is always positive, i.e., increasing CB always results in increasing LS.

Case 3 (Non-Monotone Impact): Although there *does* exist a direct relationship between the total amount of load shedding and the cleared CBs, the relationship is *not* monotone. Therefore, the sign of the *slope* of function $f(\cdot)$ in (3.19) may *vary* depending on the amount of the cleared CBs. An example for a non-monotone relationship is shown in Fig. 2(c).

While Case 1 is *not* of concern in this study, as it does *not* indicate any issue with the CBs as far as their impact on load shedding is concerned, Case 2 and Case 3 are both important and insightful and can be investigated in more details. This important analysis is conducted in Sections 3.3.1 and 3.3.2.

3.2.4 Impact of Load Shedding on CB Profit

When the network experiences load shedding, the basic formulation of the RTM optimization problem in (3.7)-(3.11) changes according to the following revised formulation:

$$\underset{\mathbf{y}}{\text{minimize}} \quad 0.5\,\mathbf{y}^T\mathbf{E}\,\mathbf{y} + \mathbf{k}^T\mathbf{y} \tag{3.21}$$

$$\text{subject to} \quad \mathbf{1}^T\mathbf{y} - \mathbf{1}^T(\mathbf{L} - \mathbf{s}^*) = 0 \tag{3.22}$$

$$-\mathbf{c} \leq \mathbf{S}(\mathbf{\Psi}\,\mathbf{y} - \mathbf{\Theta}\,(\mathbf{L} - \mathbf{s}^*)) \leq \mathbf{c} \tag{3.23}$$

$$\mathbf{x}^{\min} \leq \mathbf{y} \leq \mathbf{x}^{\max} \tag{3.24}$$

$$\mathbf{g}(\mathbf{x}^*) \leq \mathbf{y} \leq \mathbf{h}(\mathbf{x}^*) \tag{3.25}$$

where $\mathbf{s}^*$ is the optimal solution of the FSCP in (3.12)-(3.17). The above optimization problem is the basis to calculate the LMPs in the RTM. The LMPs are calculated based on the dual variables associated with the constraints in (3.21)-(3.25), c.f. [4].

Let us denote the vector of LMPs in the RTM by $\boldsymbol{\pi}^{\mathrm{RTM}}$. Similarly, let us denote the vector of LMPs in the DAM by $\boldsymbol{\pi}^{\mathrm{DAM}}$. The latter is calculated based on the dual variables associated with the constraints in the DAM optimization in (3.1)-(3.5). We can use the following vector of *price difference* to determine whether a cleared CB is *profitable* at each bus:

$$\boldsymbol{\pi}^{\mathrm{RTM}} - \boldsymbol{\pi}^{\mathrm{DAM}}. \tag{3.26}$$

If the difference is positive, then the demand CB is profitable. If it is negative, then the supply CB is profitable.

Similar to the functional relationship in Section 3.2.3, we can examine how the price difference in (3.26) may change when there is a change in CB. Since load shedding only affects the RTM, it has *no impact* on the prices in the DAM. Therefore, we only need to examine the impact of load shedding on the prices in the RTM, i.e., the impact of LS on $\boldsymbol{\pi}^{\mathrm{RTM}}$. We will discuss this subject in details in Section 3.3.3.

In summary, we seek to understand two types of relationships: 1) the impact of CBs on load shedding; 2) the impact of load shedding on the profits associated with the CBs. These two relationships will build the foundation for us to investigate the operation and the impact of CBs during power outages.

3.3 Mathematical Results

This section contains our core analytical results. First, we propose two theorems to obtain the slope of function $f(\cdot)$, as defined in (3.20), under two different operating conditions: *with* and *without* transmission line congestion in the DAM. After that, we will also examine the relationship between load shedding and the profit associated with the cleared CBs.

3.3.1 Slope of $f(\cdot)$ with No Congestion in the DAM

Suppose there is no congestion in any transmission line in the DAM. Importantly, we do *not* make any assumption regarding transmission line congestion in the RTM.

Theorem 1: If there is no congestion in the network in the DAM, then regardless of the congestion status in the RTM, the relationship between the amount of the cleared CBs and the total amount of load shedding is always *monotone*. In such monotone relationship, increasing (decreasing) the supply CB will result in more (less) load shedding. As a result, a supply (demand) CB will exacerbate (help) the power outage.

Proof of Theorem 1: Since there is no congestion in the DAM, the inequality constraints in (3.3) are eliminated. We want to calculate the *slope* of function $f(\cdot)$, which is defined in (3.20). Accordingly, we can use the infinitesimal version of the chain rule for multi-variable functions to obtain:

$$\frac{\Delta LS}{\Delta CB} = \sum_{i \in N_G} \left(\frac{\Delta LS}{\Delta h_i(x_i^*)} \cdot \frac{\Delta h_i(x_i^*)}{\Delta x_i^*} \cdot \frac{\Delta x_i^*}{\Delta CB} \right), \tag{3.27}$$

where for each generation unit i, notation x_i^* is the corresponding optimal generation schedule in the DAM optimization problem, and $h_i(x_i^*)$ is the corresponding upper bound in the inequality constraint in (3.16) in the FCSP.

There are three *fractions* in the formulation in (3.27). We claim that the following inequalities hold for these fractions:

$$\frac{\Delta LS}{\Delta h_i(x_i^*)} \leq 0, \quad \forall i \in N_G, \tag{3.28}$$

$$\frac{\Delta h_i(x_i^*)}{\Delta x_i^*} \geq 0, \quad \forall i \in N_G, \tag{3.29}$$

$$\frac{\Delta x_i^*}{\Delta CB} \leq 0, \quad \forall i \in N_G. \tag{3.30}$$

From (3.27), if these three inequalities are true, then we have:

$$\frac{\Delta LS}{\Delta CB} \geq 0. \tag{3.31}$$

In other words, if we can show that the three inequalities in (3.28)-(3.30) hold, then the proof of Theorem 1 is complete.

First, consider the inequality in (3.28). The fraction in this inequality captures the sensitivity of the optimal objective value in the FCSP in (3.12)-(3.17) with respect to the upper-bound parameter in the inequality constraint in (3.16). Since FCSP is a *minimization* problem, and also because increasing $h_i(x_i^*)$ results in *relaxing* the constraint in (3.16), we can conclude that increasing $h_i(x_i^*)$ cannot result in increasing the optimal objective value in FCSP. In other words, if $\Delta h_i(x_i^*) \geq 0$, then $LB \leq 0$. Thus, the inequality in (3.28) is indeed true.

Next, consider the inequality in (3.29). It is the direct result of the fact that, for each generator i, function $h_i(\cdot)$ is non-decreasing; as we discussed at the end of Section 3.2.1. Thus, no further proof is needed regarding the inequality in (3.29).

Finally, consider the inequality in (3.30). Verifying this inequality is *not* straightforward. It requires a detailed mathematical discussion. Therefore, for the rest of this proof, we focus on explaining why the inequality in (3.30) is true.

Given $\mathbf{x}^*$ as the optimal generation schedule in the DAM optimization problem, let us define the following three sets:

$$A = \{i \mid i \in N_G,\ x_i^{\min} \leq x_i^* \leq x_i^{\max}\}, \tag{3.32}$$

$$B = \{i \mid i \in N_G,\ x_i^* = x_i^{\min}\}, \tag{3.33}$$

$$C = \{i \mid i \in N_G,\ x_i^* = x_i^{\max}\}. \tag{3.34}$$

Similarly, given $\mathbf{z}^*$ as the optimal load schedule in the DAM optimization problem, we define the following three sets:

$$D = \{j \mid j \in N_L,\ z_j^{\min} \leq z_j^* \leq z_j^{\max}\}, \tag{3.35}$$

$$E = \{j \mid j \in N_L,\ z_j^* = z_j^{\min}\}, \tag{3.36}$$

$$F = \{j \mid j \in N_L,\ z_j^* = z_j^{\max}\}. \tag{3.37}$$

Accordingly, we can rewrite the equality in (3.2) as follows:

$$\sum_{i\in A} x_i^* + \sum_{i\in B} x_i^{\min} + \sum_{i\in C} x_i^{\max} - \sum_{j\in D} z_j^* - \sum_{j\in E} z_j^{\min} - \sum_{j\in F} z_j^{\max} + CB = 0. \tag{3.38}$$

From (3.32) and (3.35), we do *not* know the value of x_i^* for any $i \in A$, and the value of z_j^* for any $j \in D$. To obtain them, we use the Karush-Kuhn-Tucker (KKT) conditions [46]. From the KKT conditions for the DAM optimization problem in (3.1)-(3.5), excluding (3.3) due to absence of congestion, we have:

$$a_i x_i^* + b_i + \lambda_i^* - \delta_i^* + \nu^* = 0, \quad \forall i \in N_G, \tag{3.39}$$

$$-c_j z_j^* - d_j + \lambda_j^* - \delta_j^* - \nu^* = 0, \quad \forall j \in N_L, \tag{3.40}$$

where δ_i and λ_i are the Lagrange multipliers corresponding to constraint $x_i^{\min} \leq x_i$ and constraint $x_i \leq x_i^{\max}$, respectively; δ_j and λ_j are the Lagrange multipliers corresponding to constraint $z_j^{\min} \leq z_j$ and constraint $z_j \leq z_j^{\max}$, respectively; and ν is the Lagrange multiplier corresponding to the equality constraint in (3.2). As for a_i, b_i, c_j, and d_j, they are the corresponding entries in $\mathbf{A}$, $\mathbf{b}$, $\mathbf{C}$, and $\mathbf{d}$, respectively.

From (3.32) and (3.35), we have:

$$\delta_i^* = \lambda_i^* = 0, \quad \forall i \in A, \tag{3.41}$$

$$\delta_j^* = \lambda_j^* = 0, \quad \forall j \in D. \tag{3.42}$$

By replacing (3.41) in (3.39), and also by replacing (3.42) in (3.40), and after reordering the terms, we can obtain:

$$x_i^* = -(b_i + \nu^*)/a_i, \quad \forall i \in A, \tag{3.43}$$

$$z_j^* = -(d_j + \nu^*)/c_j, \quad \forall j \in D. \tag{3.44}$$

By placing (3.43) and (3.44) in (3.38), we obtain:

$$
\begin{aligned}
&-\sum_{i\in A}\frac{b_i}{a_i}-\nu^*\sum_{i\in A}\frac{1}{a_i}+\sum_{i\in B}x_i^{\min}+\sum_{i\in C}x_i^{max}\\
&\quad+\sum_{j\in D}\frac{d_j}{c_j}+\nu^*\sum_{j\in D}\frac{1}{c_j}-\sum_{j\in E}z_j^{\min}\\
&\quad-\sum_{j\in F}z_j^{max}+CB=0.
\end{aligned}
\tag{3.45}
$$

By obtaining ν^* from (3.45) and then replacing it in (3.43) for each generator $i \in A$, we can obtain:

$$
\begin{aligned}
x_i^* = -\frac{b_i}{a_i}-\frac{1}{a_i}\times\Bigg(&1/\left[\sum_{i\in A}\frac{1}{a_i}-\sum_{j\in D}\frac{1}{c_j}\right]\cdot CB\\
&+1/\left[\sum_{i\in A}\frac{1}{a_i}-\sum_{j\in D}\frac{1}{c_j}\right]\cdot\left[\sum_{i\in B}x_i^{\min}+\sum_{i\in C}x_i^{max}\right.\\
&\left.-\sum_{j\in E}z_j^{\min}-\sum_{j\in F}z_j^{max}-\sum_{i\in A}\frac{b_i}{a_i}+\sum_{j\in D}\frac{d_j}{c_j}\right]\Bigg)
\end{aligned}
\tag{3.46}
$$

Since the DAM optimization problem is a convex optimization problem, parameter $a_i \geq 0$ for all generators $i \in N_G$ and parameter $c_j \leq 0$ for all loads $j \in N_L$. Thus, we have:

$$
\sum_{i\in A}\frac{1}{a_i}-\sum_{j\in D}\frac{1}{c_j}>0. \tag{3.47}
$$

Hence, the coefficient of CB in (3.46) is always negative; and for any $i \in A$, the optimal solution x_i^* is always a decreasing function of CB. This confirms the inequality in (3.30).

In summary, the inequalities in (3.28)-(3.30) hold. Therefore, the inequality in (3.31) holds; and the proof is complete. ■

From Theorem 1, when there is no congestion in the DAM, and regardless of the congestion status in the RTM, the amount of cleared CBs has a monotone impact on the amount of load shedding. This matches **Case 2** in Section 3.2.3.

This means that, when the RTM problem is *infeasible*, i.e., when there is a need for load shedding in the RTM, the more cleared CBs in the DAM, the more load shedding in the RTM.

Therefore, if CB is positive (supply), then increasing it will result in *more load shedding*; and if CB is negative (demand), then increasing it will result in *less load shedding*.

Under the circumstances in Theorem 1, supply CBs in the DAM exacerbate load shedding in the RTM.

3.3.2 Slope of $f(\cdot)$ with Congestion in the DAM

Next, suppose there *is* transmission line congestion in the DAM. The assumption about transmission line congestion is only regarding the DAM. We do *not* make any assumption regarding transmission line congestion in the RTM.

Theorem 2: If there is transmission line congestion in the DAM, the relationship between the amount of a cleared CB and the amount of load shedding *may or may not* be monotone. That is, under some choices of the system parameters, the relationship is *not* monotone. And under some other choices of the system parameters, the relationship *is* monotone.

Proof of Theorem 2: For the purpose of this proof, we assume that congestion is exactly on *one* transmission line in the DAM. We denote the transmission line that is congested in the DAM by index k. Furthermore, we assume that exactly *one* CB is cleared in the DAM. We denote the bus where the CB is cleared by index m. The above scenario is all we need in order to derive a case under which the monotone property does *not* hold

under some choices of the system parameters, and it *does* hold under some other choices of the system parameters.

Suppose transmission line k is congested such that the *upper bound* constraint in (3.3) is binding. Every other inequality constraint in (3.3) is *not* binding. Accordingly, we can reduce (3.3) to the following *scalar* upper-bound constraint:

$$\sum_{i \in N_G} (\mathbf{S}\,\mathbf{\Psi})_{ki}\, x_i - \sum_{j \in N_L} (\mathbf{S}\,\mathbf{\Theta})_{kj}\, z_j + (\mathbf{S}\,\mathbf{\Omega})_{km}\, CB \leq c_k, \tag{3.48}$$

where $(\mathbf{S}\,\mathbf{\Psi})_{ki}$ denotes the entry at row k and column i of the matrix multiplication $\mathbf{S}\,\mathbf{\Psi}$; $(\mathbf{S}\,\mathbf{\Theta})_{kj}$ denotes the entry at row k and column j of the matrix multiplication $\mathbf{S}\,\mathbf{\Theta}$; and $(\mathbf{S}\,\mathbf{\Omega})_{km}$ denotes the entry at row k and column m of the matrix multiplication $\mathbf{S}\,\mathbf{\Omega}$. From (3.6), and because bus m is the only bus with a cleared CB in the DAM, we have $CB = v_m$.

As in Section 3.3.1, let us define $A, B, C \subseteq N_G$ as in (3.32)-(3.34) and $D, E, F \subseteq N_L$ as in (3.35)-(3.37). Since the inequality in (3.48) is binding, it holds as equality at the optimal solution. From this, together with the results in (3.32)-(3.37), we have:

$$\begin{aligned}
&\sum_{i \in A} (\mathbf{S}\,\mathbf{\Psi})_{ki}\, x_i^* + \sum_{i \in B} (\mathbf{S}\,\mathbf{\Psi})_{ki}\, x_i^{\min} \\
&\quad + \sum_{i \in C} (\mathbf{S}\,\mathbf{\Psi})_{ki}\, x_i^{max} - \sum_{j \in D} (\mathbf{S}\,\mathbf{\Theta})_{kj}\, z_j^* \\
&\quad - \sum_{j \in E} (\mathbf{S}\,\mathbf{\Theta})_{kj}\, z_j^{\min} - \sum_{j \in F} (\mathbf{S}\,\mathbf{\Theta})_{kj}\, z_j^{max} \\
&\quad + (\mathbf{S}\,\mathbf{\Omega})_{km}\, CB - c_k = 0.
\end{aligned} \tag{3.49}$$

From (3.32)-(3.37), the equality in (3.2) can be written as:

$$\sum_{i\in A} x_i^* + \sum_{i\in B} x_i^{\min} + \sum_{i\in C} x_i^{max} - \sum_{j\in D} z_j^* - \sum_{j\in E} z_j^{\min} - \sum_{j\in F} z_j^{max} + CB = 0. \tag{3.50}$$

Based on (3.32) and (3.35), we do not know the value of x_i^* when $i \in A$ and the value of z_j^* when $j \in D$. In order to obtain these unknowns, we can use the following KKT conditions corresponding to the DAM optimization problem in (3.1)-(3.5):

$$a_i x_i^* + b_i + \lambda_i^* - \delta_i^* + \nu^* + (\mathbf{S}\,\mathbf{\Psi})_{ki}\,\theta^* = 0, \forall i \in N_G, \tag{3.51}$$

$$-c_j z_j^* - d_j + \lambda_j^* - \delta_j^* - \nu^* - (\mathbf{S}\,\mathbf{\Theta})_{kj}\,\theta^* = 0, \forall j \in N_L, \tag{3.52}$$

where δ_i and λ_i are the Lagrange multipliers corresponding to constraint $x_i^{\min} \le x_i$ and constraint $x_i \le x_i^{\max}$, respectively; δ_j and λ_j are the Lagrange multipliers corresponding to constraint $z_j^{\min} \le z_j$ and constraint $z_j \le z_j^{\max}$, respectively; ν is the Lagrange multiplier corresponding to the equality constraint and θ is the Lagrange multiplier corresponding to the upper-bound transmission line constraint in (3.48).

From (3.32), (3.35), (3.51), and (3.52), we can obtain:

$$x_i^* = -(b_i + \nu^* + (\mathbf{S}\,\mathbf{\Psi})_{ki}\,\theta^*)/a_i, \quad \forall i \in A, \tag{3.53}$$

$$z_j^* = -(d_j + \nu^* - (\mathbf{S}\,\mathbf{\Theta})_{kj}\,\theta^*)/c_j, \quad \forall j \in D. \tag{3.54}$$

Next, for notational simplify, we define:

$$t_1 := -\sum_{i\in A}\frac{b_i}{a_i}+\sum_{j\in D}\frac{d_j}{c_j} + \sum_{i\in B}x_i^{\min}+\sum_{i\in C}x_i^{max}-\sum_{j\in E}z_j^{\min}-\sum_{j\in F}z_j^{max} \tag{3.55}$$

$$t_2 := -\sum_{i\in A}\frac{(\mathbf{S}\,\mathbf{\Psi})_{ki}b_i}{a_i}+\sum_{j\in D}\frac{(\mathbf{S}\,\mathbf{\Theta})_{kj}d_j}{c_j} + \sum_{i\in B}(\mathbf{S}\,\mathbf{\Psi})_{ki}\,x_i^{\min}+\sum_{i\in C}(\mathbf{S}\,\mathbf{\Psi})_{ki}\,x_i^{max} - \sum_{j\in E}(\mathbf{S}\,\mathbf{\Theta})_{kj}\,z_j^{\min}-\sum_{j\in F}(\mathbf{S}\,\mathbf{\Theta})_{kj}\,z_j^{max}-c_k. \tag{3.56}$$

By replacing (3.53) and (3.54) in (3.50), we can obtain:

$$\nu^*\left(\sum_{j\in D}\frac{1}{c_j}-\sum_{i\in A}\frac{1}{a_i}\right)-\theta^*\left(\sum_{i\in A}\frac{(\mathbf{S}\,\mathbf{\Psi})_{ki}}{a_i} +\sum_{j\in D}\frac{(\mathbf{S}\,\mathbf{\Theta})_{kj}}{c_j}\right)+CB+t_1=0. \tag{3.57}$$

By replacing (3.53) and (3.54) in (3.49), we can obtain:

$$\nu^*\left(\sum_{j\in D}\frac{(\mathbf{S}\,\mathbf{\Theta})_{kj}}{c_j}-\sum_{i\in A}\frac{(\mathbf{S}\,\mathbf{\Psi})_{ki}}{a_i}\right)-\theta^*\left(\sum_{i\in A}\frac{((\mathbf{S}\,\mathbf{\Psi})_{ki})^2}{a_i} +\sum_{j\in D}\frac{((\mathbf{S}\,\mathbf{\Theta})_{kj})^2}{c_j}\right)+(\mathbf{S}\,\mathbf{\Omega})_{km}\,CB+t_2=0. \tag{3.58}$$

In (3.57), let us refer to the coefficient of ν^* as g_1 and the coefficient of θ^* as g_2. Similarly, in (3.58), let us refer to the coefficient of ν^* as g_3, the coefficient of θ^* as g_4, and the coefficient of CB as g_5. Accordingly, we can express (3.57) and (3.58) in the following simplified forms:

$$\nu^* g_1-\theta^* g_2+CB+t_1=0 \tag{3.59}$$

$$\nu^* g_3-\theta^* g_4+g_5\,CB+t_2=0, \tag{3.60}$$

respectively. By solving the system of linear equations in (3.59) and (3.60), we can express ν^* and θ^* as a function of CB. After that, we can replace the results in (3.53) to obtain:

$$\frac{\Delta x_i^*}{\Delta CB} = -\frac{1}{a_i} \times \left(\frac{g_4 - g_2 g_5}{g_2 g_3 - g_1 g_4} \right) - \frac{(\mathbf{S}\,\mathbf{\Psi})_{ki}}{a_i} \times \left(\frac{g_3 - g_1 g_5}{g_2 g_3 - g_1 g_4} \right). \tag{3.61}$$

The sign of the above equation can change depending on the choice of the parameters in the system. Based on the values of g_1, g_2, g_3, g_4, and g_5, it is possible that the inequality in (3.30) holds; which in that case, the inequality in (3.31) will hold. In that case, the relationship between the amount of the cleared CB in the DAM and the amount of load shedding in the RTM *is* monotone. Based on the values of g_1, g_2, g_3, g_4, and g_5, it is possible that the inequality in (3.30) does *not* hold, to the extent that the inequality in (3.31) does *not* hold either; which means the relationship between the amount of the cleared CB in the DAM and the amount of load shedding in the RTM is *not* monotone. We will see examples of both scenarios, i.e., both monotone and non-monotone cases, in Section 3.4. ■

From Theorem 2, when there is transmission line congestion in the DAM, and regardless of the congestion status in the RTM, it is possible for the relationship between the amount of cleared CBs and the amount of load shedding to be monotone, as in **Case 2** in Section 3.2.3; or non-monotone, as in **Case 3** in Section 3.2.3. It all depends on the values of the parameters.

In practice, when there is congestion in the DAM, in order to specify which CB will exacerbate the power outage and which CB will heal the power outage, the ISO needs

to calculate the values of parameters g_1, g_2, g_3, g_4, and g_5 to determine the sign of the expression on the right-hand-side in (3.61).

Importantly, as we will see in the numerical case studies in Section 3.4, the relationship between a cleared CB in the DAM and the load shedding in the RTM is *most often* monotone. In other words, even under the circumstances in Theorem 2, the results are *most often* similar to the results in Theorem 1.

3.3.3 Relationship between Load Shedding and CB Profit

Recall from Section 3.2.4 that, since load shedding only affects the RTM, it does not affect the LMPs in the DAM. From this, together with the formulation of the price difference in (3.26), in order to examine the impact of load shedding on CB profit, we only need to examine how $\boldsymbol{\pi}^{\mathrm{RTM}}$ changes when LS changes. Accordingly, we can present two theorems.

Theorem 3: If there is no congestion in the network in the RTM, then the relationship between the amount of the load shedding and the profit of the CBs is always monotone. In such monotone relationship, increasing (decreasing) the amount of load shedding will result in more (less) profit for supply (demand) CBs; as a result, a supply (demand) CB will be advantaged (disadvantaged) by the power outage.

Proof of Theorem 3: When there is no transmission line congestion in the RTM, the LMP at any bus in the RTM is equal to the dual variable associated with the power balance constraint in (3.22), c.f. [4]. Let us define such dual variable by π^{RTM}; where $\boldsymbol{\pi}^{\mathrm{RTM}} = \pi^{\mathrm{RTM}}\mathbf{1}$. Accordingly, we are concerned with obtaining the sign of the following

fraction:

$$\frac{\Delta\pi^{\text{RTM}}}{\Delta LS}. \tag{3.62}$$

From (3.18), we can rewrite (3.22) as $\mathbf{1}^T\mathbf{y} - \mathbf{1}^T\mathbf{L} = LS$; thus LS is a parameter in the equality constraint in (3.22). Let Obj^* denote the optimal objective value of the RTM optimization problem in (3.21)-(3.25). From the subject of *perturbation and sensitivity analysis* in convex optimization, we know that [49]:

$$\pi^{\text{RTM}} = -\frac{\Delta Obj^*}{\Delta LS}. \tag{3.63}$$

Therefore, by applying the infinitesimal version of the definition of derivative, we can express the fraction in (3.63) as:

$$\frac{\Delta\pi^{\text{RTM}}}{\Delta LS} = -\frac{\Delta\left(\Delta Obj^*/\Delta LS\right)}{\Delta LS} = -\frac{\Delta^2 Obj^*}{\Delta LS^2}, \tag{3.64}$$

where the last fraction is the infinitesimal version of the definition of the *second derivative*. Since the RTM optimization problem in (3.21)-(3.25) is convex, its objective function is convex and has a *non-negative second derivative* [49]. From this, together with the results in (3.64), we can conclude that:

$$\frac{\Delta\pi^{\text{RTM}}}{\Delta LS} \leq 0. \tag{3.65}$$

From (3.65) and (3.26), and since load shedding does not affect the prices in the DAM, we can conclude that, the CB profit is a monotone function of the amount of load shedding.

■

From Theorem 3, increasing load shedding during power outages results in increasing the profit for supply CBs and decreasing the profit for demand CBs. This monotone

relationship is guaranteed if there is *no* transmission line congestion in the RTM. If there *is* transmission line congestion in the RTM, then we can present the following theorem.

Theorem 4: If there is transmission line congestion in the RTM, then the relationship between the amount of the load shedding and the profit of the CBs *may or may not* be monotone. Under some choices of the system parameters, the relationship is *not* monotone. And under some other choices of the system parameters, the relationship *is* monotone.

The above theorem is the direct result of the concept of negative injection shift factors in the analysis of LMPs; a concept that is extensively studied in the literature [50,51]. However, similar to the case in Theorem 2, having a non-monotone relationship is rare; as we will also see through case studies in Section 3.4.2 and Section 3.5.2.

3.3.4 Summary of the Mathematical Results

From Theorem 1 and Theorem 3, if there is no transmission line congestion in the system, then we can identify the following issue in the operation of CBs during power outages:

The Issue: On one hand, supply CBs exacerbate the power outage by increasing the required amount of load shedding, while demand CBs heal the power outage by decreasing the required amount of load shedding. On the other hand, load shedding creates advantage for supply CBs by increasing their profit, while it creates disadvantage for demand CBs by decreasing their profit. This situation can be unfair; because it rewards the type of CBs that exacerbate power outages and punishes the type of CBs that heal power outages.

From Theorem 2 and Theorem 4, if there is transmission line congestion in the system, then the above issue may not necessary hold. However, as we will see in Section 3.4, the monotone relationship between the cleared CBs and the amount of load shedding, as well as the monotone relationship between the amount of load shedding and the CB profit are most often monotone. Thus, the above issue most often does hold. In fact, it appears that the above issue was behind a decision by the California ISO to entirely suspend CBs during the outages in August 2020, as we will discuss in Section 3.5.

3.4 Numerical Case Studies

In this section, we verify the mathematical results in Section 3.3 through numerical case studies. All the numerical case studies are based on the IEEE 14-bus test system, as shown in Fig. 3.2. There are five generation units and ten consumption units in the system. The basic characteristics of the generation units, consumption units, and transmission lines are as in [52]. We consider nominal load at each bus in the IEEE 14-bus test system as the self-scheduling load in the DAM at that bus. In the RTM, we assume that there is 25% increase in the actual load compared to the DAM schedule. The capacity of each transmission line is 45 MW. For the five generation units, we have: $\mathbf{A} = \text{diag}(3, 2, 1, 1, 2)$ and $\mathbf{b} = [15, 10, 14, 14, 10]$. The maximum generation capacity for each generation unit is 100 MW. We assume that, the generation units use the same bids in the RTM as in the DAM, i.e., $\mathbf{E} = \mathbf{A}$ and $\mathbf{k} = \mathbf{b}$.

Regarding the choice of the functions $\mathbf{g}(\cdot)$ and $\mathbf{h}(\cdot)$ in (3.11), we assume that the actual output of the first three generation units in the RTM have the following dependencies

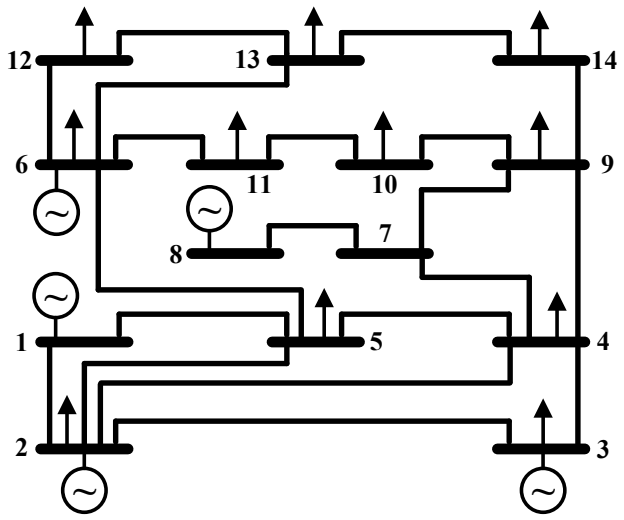

Figure 3.2: The IEEE 14-bus standard test system that is studied in Section 3.4.

to their optimal DAM schedule: (i) the generation unit at bus 1 cannot increase its actual output more than 30% of its DAM schedule, i.e., for this generation unit, we have: $h(x^*) = 1.3\,x^*$; (ii) the generation unit at bus 2 cannot increase its actual output more than 10% of its DAM schedule, and it cannot reduce its generation output in the RTM to a level less than its DAM schedule, i.e., for this generation unit, we have: $h(x^*) = 1.1\,x^*$ and $g(x^*) = x^*$; (iii) the generation unit at bus 3 cannot increase its actual output more than 20% of its DAM schedule, i.e., for this generation unit, we have: $h(x^*) = 1.2\,x^*$.

3.4.1 Relationship between Load Shedding and Cleared CB

In order to *numerically* obtain function $f(\cdot)$ in (3.19), we change the amount of the CB at a given bus in the DAM within a certain range, and we accordingly solve the DAM optimization problem in (3.1)-(3.5), the RTM optimization problem in (3.7)-(3.11),

and the feasibility check subproblem in (3.12)-(3.17) to obtain the resulting load shedding in the RTM.

We analyze three different cases, as listed below. Case A matches the mathematical results in Theorem 1. Case B and Case C match the mathematical results in Theorem 2.

Case A (No Congestion - Monotone Behavior): The results in this case are shown in Fig. 3.3. Notice that the load shedding is a *monotone increasing* function of the supply CB and a *monotone decreasing* function of the demand CB. To plot these curves, first, we examine a supply CB at an amount that increases from 0 MW to 10 MW. This results in obtaining the green curve. Next, we examine a demand CB at an amount that increases from 0 MW to 10 MW. This results in obtaining the red curve. One could interpret the results in Fig. 3.3 also in terms of changing the CB from -10 MW (demand) to $+10$ MW (supply). In that case, the combined load shedding curve would be *monotone increasing*. The numerical results in Fig. 3.3 match the mathematical results in Theorem 1.

Importantly, as we can see in Fig. 3.3, a supply CB *exacerbates* the power outage by increasing the required amount of load shedding; while a demand CB *heals* the power outage by decreasing the required amount of load shedding.

Case B (Congestion - Monotone Behavior): The results in this case are shown in Fig. 3.4. The capacity of the transmission lines is 20% less than those in Case A. Accordingly, there *is* transmission line congestion in the DAM in this case. Notice that, at *all* buses, the curves in Fig. 3.4 are *monotone* functions. The numerical results in Fig. 3.4 match the mathematical results in Theorem 2. In particular, recall from Theorem 2 that

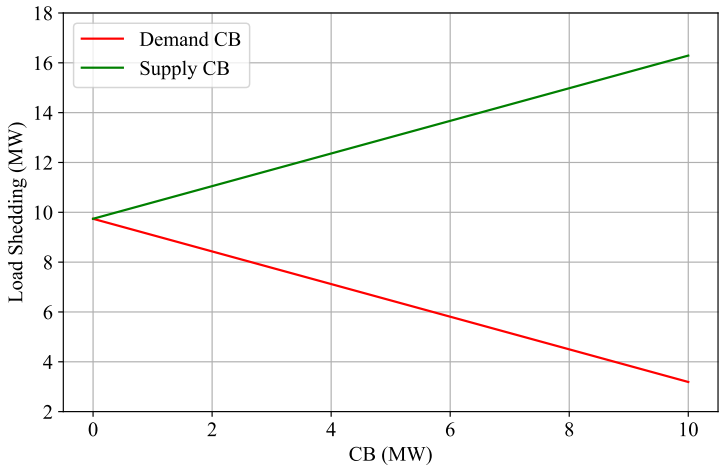

Figure 3.3: The numerical results in **Case A**: load shedding as a *monotone* function of a supply CB (green curve) and a demand CB (red curve). There is *no* transmission line congestion in the DAM. The results match Theorem 1.

even if some of the transmission lines are congested in the DAM, it is possible that the load shedding in the RTM is a monotone function of the cleared CB at any bus. In this figure, we only see the curves for two buses in the system. The curves for the rest of the buses are not shown; because they simply match one of the curves that are already shown in this figure.

For all the buses in Fig. 3.4, a supply CB *exacerbates* the power outage by increasing the required amount of load shedding; while a demand CB *heals* the power outage by decreasing the required amount of load shedding. Therefore, the ultimate outcome in Case B is similar to Case A, despite having congestion in the transmission lines in the DAM.

Case C (Congestion - Non-Monotone Behavior): The results in this case are shown in Fig. 3.5. The capacity of the transmission lines is 35% less than those in Case A and there *is* transmission line congestion in the DAM.

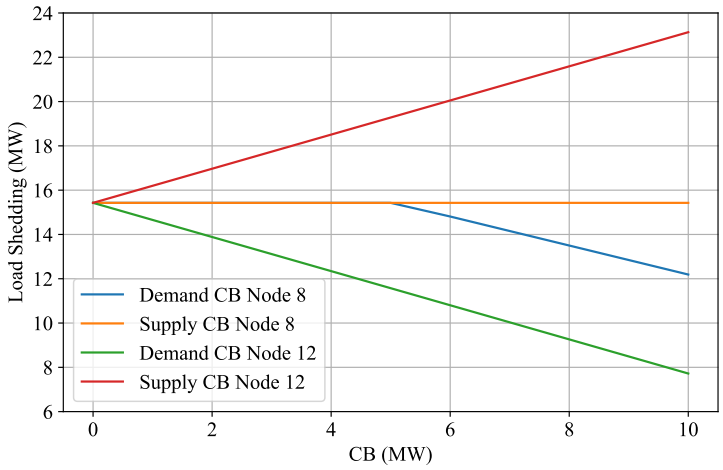

Figure 3.4: The numerical results in **Case B**: load shedding as a *monotone* function of supply CB at difference buses (red and orange curves) and demand CB at different buses (green and blue curves). There *is* transmission line congestion in the DAM. The capacity of the transmission lines are 20% less than those in Case A. The results match Theorem 2.

Fig. 3.5(a) shows the total load shedding as a function of the cleared CBs at buses 3, 8, and 12. Notice that, all the curves in Fig. 3.5(a) are monotone. A supply CB at any of these three buses *exacerbates* the power outage while a demand CB *heals* the power outage. Importantly, the monotone behavior that is shown in Fig. 3.5(a) holds not only at buses 3, 8, and 12, but also at every other bus, *except* at bus 5; as we will see next.

Fig. 3.5(b) shows the total load shedding as a function of the cleared CB at bus 5. We can see that the load shedding is *not* a monotone function of the cleared supply CB at bus 5. This scenario is very rare, but it does happen in this case.

Next, we discuss the non-monotone behavior in Fig. 3.5(b), when the supply CB at bus 5 is between 0 MW to 4 MW. The added CB causes congestion in the DAM on the line between bus 4 and bus 5. Due to this new congestion, the generation schedule for the generator at bus 3 in the DAM increases (instead of decreasing). Since the output of this unit in the RTM depends on its DAM schedule, this generator will have more output in the

RTM when a supply CB is placed at bus 5 which causes a decrease in the amount of load shedding. This causes the non-monotone behavior in Fig. 3.5(b), for the range of supply CB between 0 to 4 MW. Ultimately, by increasing the supply CB beyond 4 MW, the output of the generator at bus 3 reaches its maximum physical capacity in the RTM. As a result, its generation output in the RTM is no longer dependent on its DAM schedule. Accordingly, a supply CB at bus 5 that is larger than 4 MW causes the same typical monotone effect on the load shedding that we saw in Cases A and B.

The numerical results in Fig. 3.5 match the mathematical results in Theorem 2. It is worth emphasizing that, the above non-monotone behavior is very rare and it happens only under some very specific circumstances, as we discussed in Theorem 2. In most cases, the monotone behavior *does* hold; but there do exist cases for which the monotone behavior does not hold. As mentioned in Theorem 2, such rare cases can happen only if there is transmission line congestion in the DAM.

3.4.2 Relationship between Load Shedding and CB Profit

In Theorem 3 in Section 3.3.3, we mathematically proved that if there is no transmission line congestion in the RTM, load shedding *always* results in decreasing (increasing) the profit of demand (supply) CBs. Therefore, we do not provide any numerical result for the case in Theorem 3. Instead, in this section, we numerically obtain the relationship between load shedding and the profit of CBs in the presence of congestion in the RTM. For this purpose, we use the same setting that we introduced in the beginning of Section 3.4. The results are shown in Fig. 3.6. Here, we gradually shed the load at bus 3, to examine

the CB profit for placing 1 MWh demand CBs at two different buses. But 3 is selected for load shedding; because it has the largest load in the system. The profit of a supply CB would be exactly the opposite in each case. As we can see, in both cases, the relationship between the amount of load shedding and the profit of the CB is monotone. Increasing the amount of load shedding results in decreasing the profit of the demand CB. It should be emphasized that the same result are achieved at any other bus in the system. This is despite the fact that there is transmission line congestion in the system.

3.5 Real-World Case Study

In this section, we discuss a real-world case study related to the power outages that happened in California in the United States due to a major heat wave during August 2020. We analyze the real-world data that is made available by the California ISO in order to analyze different aspects related to the operation and impact of CBs during this case study.

3.5.1 Overview of the Case

During August 14, 2020 through August 19, 2020, the state of California experienced a statewide extreme heat wave, which significantly increased the load for 32 million California residents due to the excessive operation of the air conditioning units. The increased stress on the electric power system resulted in a series of rotating blackouts that caused power outages for over 350,000 costumers [53]. Fig. 3.7 shows the hourly number of

costumers who lost power during the month of August [54]. In this figure, the two spikes show the outages that happened during the peak hours:

- 6:00 PM - 9:00 PM on August 14;
- 6:00 PM - 8:00 PM on August 15.

After that, the amount of load shedding gradually decreased, although the number of customers who experienced a power outage remained higher than usual for the next several days.

In this case study, we focus on the analysis of CBs in the aggregated pricing nodes (APnodes) in the California ISO market. In August 2020 and *before* the event, i.e., from August 1 through August 13, a total of 427 APnodes hosted at least one CB at any time during this period. A total of 66 market participants submitted at least one CB to the California ISO market during this period. The total number of submitted CBs was 119,332; out of which 56% were cleared in the market.

Of interest among the APnodes in California are the three Default Load Aggregation Points (DLAPs): Pacific Gas and Electric (PG&E), Southern California Edison (SCE), and San Diego Gas and Electric (SDG&E). These three APnodes cover Northern, Central and Southern part of California. Since the LMPs at DLAPs are less volatile than the LMPs at the regular APnodes, DLAPs are desirable for submitting CBs [41].

3.5.2 Convergence Bids: Analysis of the Prices and the Profits

Fig. 3.8 shows the hourly LMPs during August 14 in each of the three DLAPs in the California ISO market: PG&E, SCE, and SDG&E. Both the DAM LMPs and the RTM LMPs are shown here. The vertical lines in each figure show the start time and the end time of the period of power outage (i.e., severe load shedding). As we can see in this figure, in all the three cases, we can distinguish two different periods. At the beginning, and up until the start of the outage period, the RTM LMP is *higher* than the DAM LMP; because the network is experiencing a higher load in real-time than expected. However, right around the time that the California ISO started dispatching severe load shedding, the RTM LMPs *suddenly started to drop* and became *lower* than the DAM LMPs.

The exact same situation also happened on August 15, 2020, as soon as the ISO started dispatching the load shedding across the system. The figures are not shown here.

From the above observations, while the demand CBs made profit before the outages, they started losing money as soon as the outages started. This exactly matches our analysis in Section 3.3.3. Furthermore, this matches the concern that we raised in Section 3.3.4; because the demand CBs, which are the type of CBs that help healing the power outages, are actually being negatively affected by the power outages. In other words, they are punished instead of being rewarded.

Next, we examine and compare the profit that is gained by each cleared CB during two different market conditions:

- **During Peak Outage Hours:** From 6:00 PM to 9:00 PM on August 14 and also from 6:00 PM to 8:00 PM on August 15. The results are shown in Fig. 3.9(a).

- **Right Before Peak Outage Hours:** From 3:00 PM to 6:00 PM on August 14 and also from 4:00 PM to 6:00 PM on August 15. The results are shown in Fig. 3.9(b).

Notice that, the results in Fig. 3.9(a) and those in Fig. 3.9(b) are the *opposite of each other*. In Fig. 3.9(a), 80% of the supply CBs have *positive* profit; while in Fig. 3.9(b), 90% of the supply CBs have *negative* profit. Furthermore, in Fig. 3.9(a), 89% of the demand CBs have *negative* profit; while in Fig. 3.9(b), 78% of the demand CBs have *positive* profit.

The above results are very insightful and they confirm some of the issues that we raised in Section 3.3.4. To see this, recall from Sections 3.3.1 and 3.3.2 that in most cases, a supply CB exacerbates the outage circumstances while a demand CB heals the outage circumstances. Accordingly, one would expect that a supply CB is punished during the outages while a demand CB is rewarded during the outages. However, that is *not* the case in practice. In fact, the occurrence of the outages creates a situation that the supply CBs are rewarded while the demand CBs are punished, instead of the opposite.

It is worth noting that, the California power system was under stress even before the outage period in Fig. 3.9(b); because the heat wave had already started. However, it had not gone to the level to cause power outages; as in the case in Fig. 3.9(a).

In summary, while load shedding is an inevitable remedial action when the power system is under stress, it has a negative impact on the electricity market, when it comes to the CBs. This matches our analysis in Sections 3.3.4 and 3.4.2.

3.5.3 Convergence Bids: Response of the ISO

The real-world results in Section 3.5.2 confirm "the issue" that we explained through mathematical analysis in Section 3.3.4. On one hand, the supply CBs in the DAM almost always result in exacerbating the power outages in the RTM by increasing the required amount of load shedding; on the other hand, increasing load shedding results in reducing the prices in the RTM; thus, unfairly rewarding the supply CBs and unfairly punishing demand CBs. This raises the question on *how should the ISO respond to such circumstances?*

Importantly, during the period from August 18 till August 21, i.e., shortly after the severe power outages, CBs were *entirely suspended* in the California ISO market. CBs were permitted again after August 21, i.e., after the level of outages almost returned to its normal level, as we saw in Fig. 3.7.

Fig. 3.10 shows all the cleared CBs in the California ISO market during the month of August. A total of 81 CB market participants had at least one cleared bid in August 2020; and each color in this figure is associated with one of the market participants. As we can see, there is no cleared CB during August 18 to August 21, as convergence bidding was fully suspended for the entire day on these four days.

It should be emphasized that the California ISO has the authority to suspend CBs when necessary per Tariff Section 7.9. This can be performed to bids already submitted or to bids that will be submitted in the future at any node [55].

While the reasoning for the California ISO's decision about suspending the CBs is *not* disclosed in details, e.g., see [53], this real-world decision *does* very well match our conclusions that we obtained mathematically in Sections 3.3 and 3.4.

3.6 Conclusions

This study addressed the open problem of understanding the operation and impact of CBs during blackouts. A new functional method as well a new metric was introduced to determine if a cleared CB is exacerbating or healing the blackout. A series of mathematical theorems were developed and numerical analysis were conducted. It was shown that, when there is no congestion in the DAM, and even most often when there is congestion in the DAM, supply CBs hurt the system during blackouts while demand CBs help the system. The impact of load shedding on the profit of CBs was also investigated in this study. The analysis in this part was again both analytical and numerical. It was shown that, load shedding usually creates advantage for supply CBs and disadvantage for demand CBs in terms of their profit. The combination of these various results raised the issue on whether the operation of CBs is fair and justified during the blackouts. Therefore, to gain more insights, we also analyzed the real-world market data from the California ISO during the blackouts in August 2020. It was shown that, the decision by the California ISO to suspend CBs during this event is justified and it matches the mathematical and numerical results that were obtained in this study.

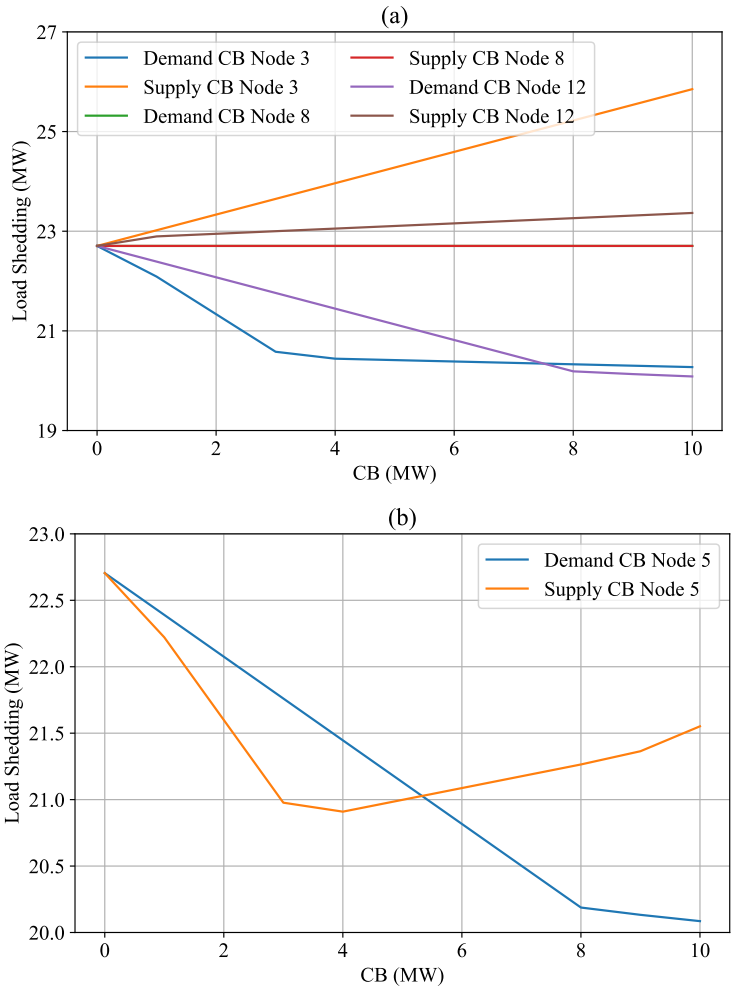

Figure 3.5: The numerical results in **Case C**: (a) load shedding as a *monotone* function of supply and demand CBs at buses 3, 8, and 12; (b) load shedding as a *non-monotone* function of supply CBs and *monotone* function of demand CBs at bus 5. There *is* transmission line congestion in the DAM. The capacity of the lines is 35% less than those in Case A. The results match Theorem 2.

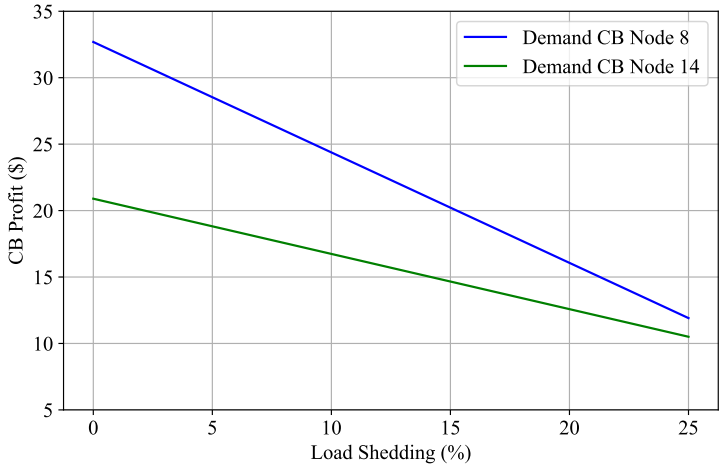

Figure 3.6: Impact of load shedding on the profit of CBs at buses 8 and 14.

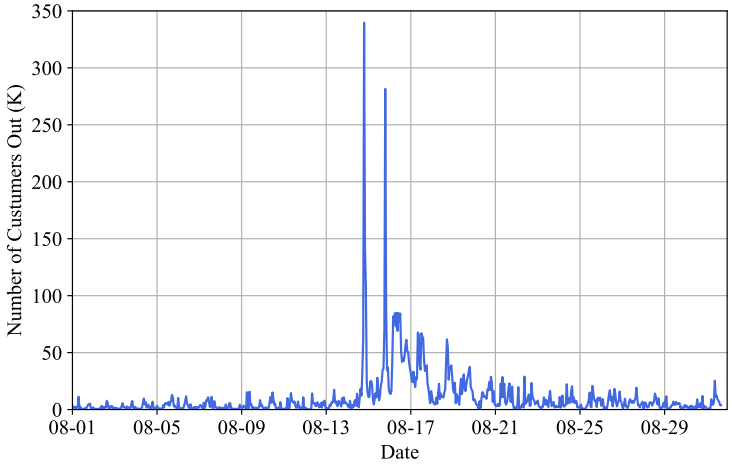

Figure 3.7: Hourly number of costumers who lost power during the month of August in the California ISO. The spikes occur on August 14 and 15.

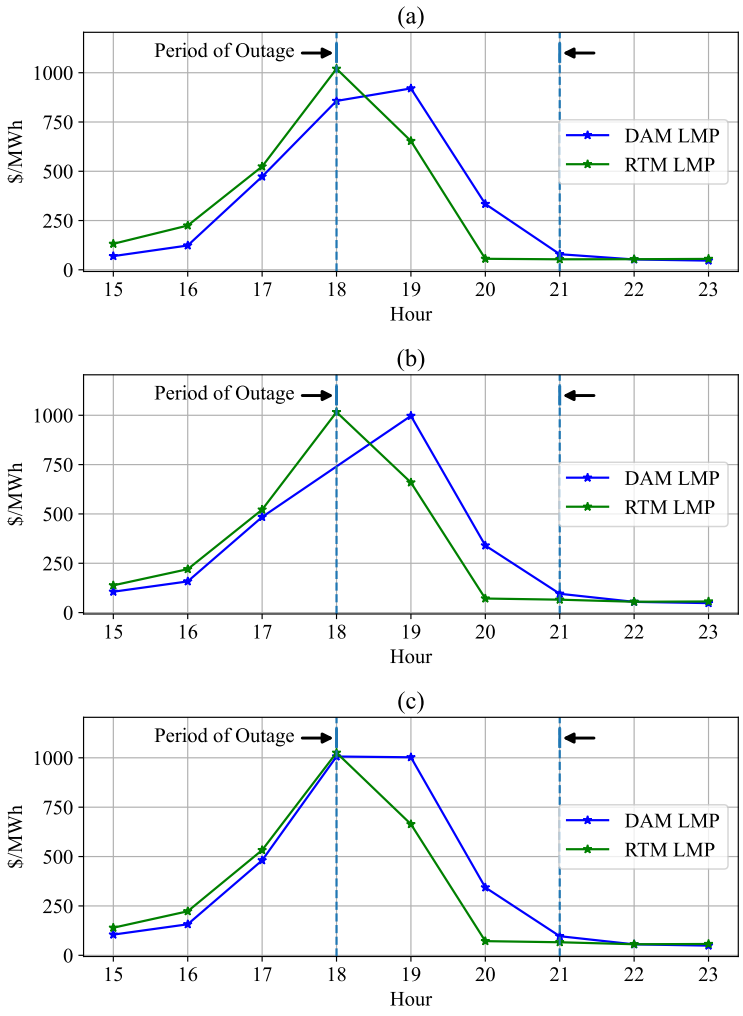

Figure 3.8: Comparing the hourly DAM LMPs and the hourly average RTM LMPs on August 14 in three DLAP in California: a) PG&E; b) SCE; c) SDG&E.

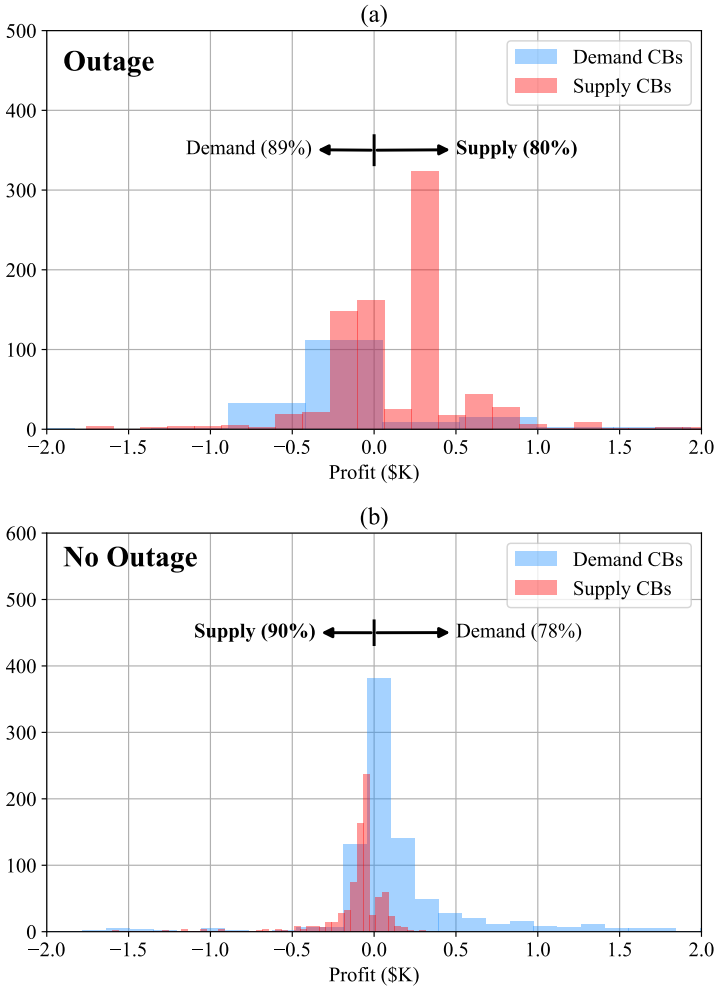

Figure 3.9: Comparing the distribution of the CB profits on August 14 and August 15 during (a) the outage hours; (b) same duration but before the outage hours.

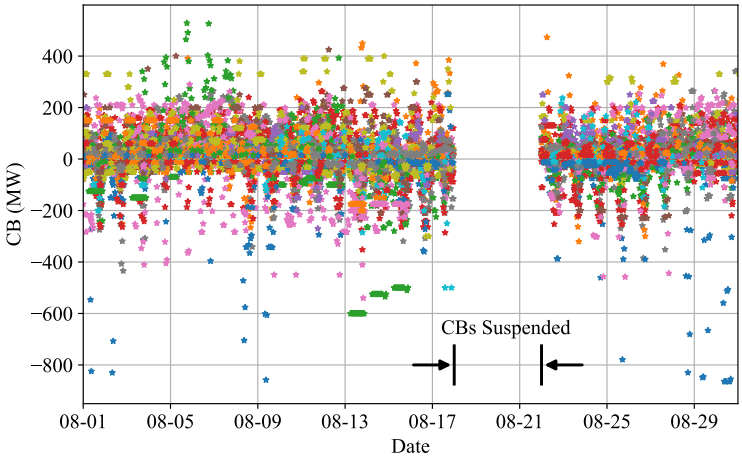

Figure 3.10: Hourly cleared CBs in August 2020 in the California ISO market. CBs were *suspended* during August 18 to August 21.

Chapter 4

Other Collaborative Research Efforts

Chapters 1, 2, and 3 are the core of this dissertation. They are based on the work that is directly related to convergence bids. They are also all led by myself. However, throughout my PhD I also worked on some collaborative projects, both on the subject of convergence bids and also on other subjects. Accordingly, in this chapter, I provide a brief summary of two other research efforts that I have been involved with during my doctoral research. I served as the second author in the first work, see Section 4.1 and [4]. I served as the first author in the second work, see Section 4.2 and [56].

4.1 Understanding the structural characteristics of convergence bidding in nodal electricity markets

As it is mentioned before, convergence bidding is a market mechanism that is used by the ISOs to increase market efficiency in electricity markets by *closing the gap* between the DAM prices and the RTM prices. However, some recent reports by ISOs have questioned whether CBs act as intended [57]. Motivated by such reports, this section and its corresponding paper in [4] provides a methodology to identify under what conditions a CB results in price divergence, instead of price convergence. The analysis is done in nodal electricity markets and factors such as *transmission line congestion* are investigated. It is proved that, under some transmission lines congestion configurations, price convergence is guaranteed. In contrast, there are certain transmission lines congestion configurations that can result in price divergence when CBs are submitted at certain nodes. Importantly, the analysis in this study also covers the stochastic case, where we obtain the *probability* of price convergence (or divergence) when we are uncertain about some system parameters.

4.1.1 Sensitivity Analysis of DAM and RTM Prices to Convergence Bids

In this analysis, the DAM and the RTM optimization problems are similar to the ones we introduced in Chapter 3. Three illustrative examples are presented to demonstrate the fundamental concepts that we seek to investigate. All three examples here are based on the three-bus network in Fig. 4.1. Generators G_1 and G_3 participate in both the DAM and RTM, while generator G_2 participates only in the RTM. In all cases, a supply CB is placed at bus 2. In Examples 1 and 2, the demand entity at Bus 2 submits a self-schedule demand

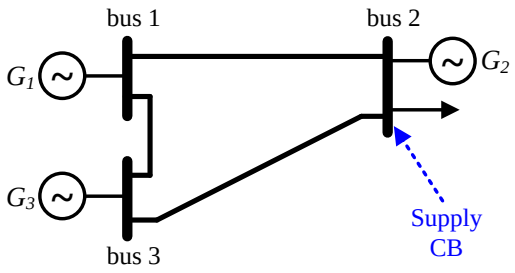

Figure 4.1: The three-bus power network that is studied in this section.

bid at 75 MWh to the DAM and its actual demand in the RTM turns out to be 90 MWh. In Example 3, we use the wind generation data from [58] and the load data from [59] to generate 150 scenarios for the net load. The other additional details are provided in the corresponding paper in [4].

Example 1 - No Congestion: Suppose all transmission lines have infinite capacity; thus, no transmission line can be congested. Accordingly, LMP is the same at all buses. If no CB is submitted to the market, i.e., when the CB is zero, then the cleared market prices in the DAM and RTM are obtained as $\boldsymbol{\pi}_1 = \boldsymbol{\pi}_2 = \boldsymbol{\pi}_3 = \$20.72$ and $\boldsymbol{\sigma}_1 = \boldsymbol{\sigma}_2 = \boldsymbol{\sigma}_3 = \$14.67$. Consider the diagrams in Fig. 4.2(a). As we increase the size of the supply CB at bus 2, the prices in the DAM increase while the prices in the RTM decrease; thus, resulting in *convergence* between the market prices. This is what is intended for a CB.

Example 2 - Congestion: Next, suppose the capacity of the transmission line between buses 1 and 2 is 47 MW. In the absence of CBs, no line is congested in the DAM and $\boldsymbol{\pi}_1 = \boldsymbol{\pi}_2 = \boldsymbol{\pi}_3 = \$20.72$. However, the transmission line between buses 1 and 2 is congested at the RTM. Accordingly, the RTM LMPs will be $\boldsymbol{\sigma}_1 = \$10.29$, $\boldsymbol{\sigma}_2 = \$19.03$, and

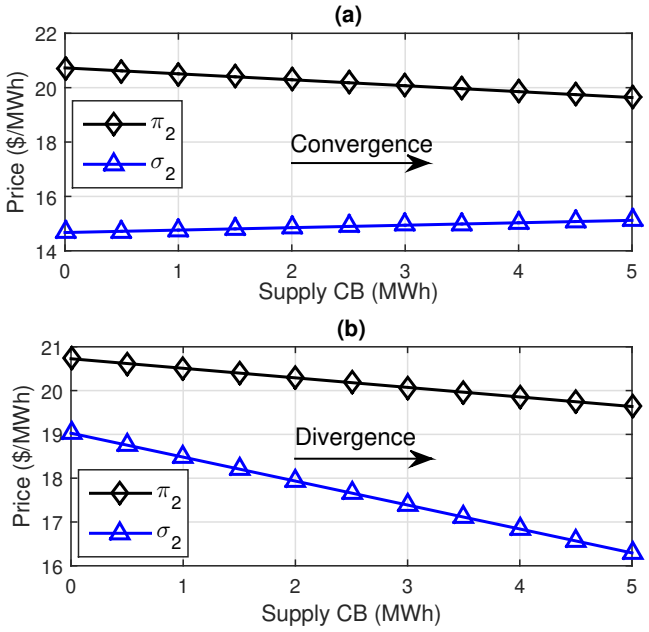

Figure 4.2: The DAM price π and the RTM price σ at Bus 2 versus the cleared energy of a supply CB at the same bus: (a) Example 1, (b) Example 2.

$\boldsymbol{\sigma}_3 = \$14.66$. Consider the diagrams in Fig. 4.2(b). As we increase the size of the supply CB at bus 2, the prices in both the DAM and RTM decrease; however the rate of decreasing is higher for the prices in the DAM. Thus results in *divergence* in the market prices. This is the opposite of what is intended for a CB.

Example 3 - Stochastic Parameters: The observations that we made in Examples 1 and 2 are fundamental. In particular, even if the parameters of the system are stochastic, we can still observe both price convergence and price divergence. To see this, suppose generator G_2 at bus 2 is replaced with a wind farm and a load, which together form a *random net load* that follows a scenario-based probability distribution. The minimum, maximum and average of the net load is 2.05 MWh, 94.11 MWh, and 63.44 MWh, respectively. The average net load is used in the DAM and the actual scenarios are used in

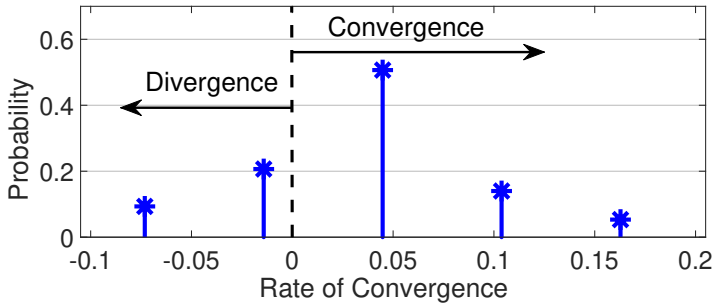

Figure 4.3: The probability distribution of the rate of convergence between the DAM and RTM prices under the random scenarios in Example 3.

the RTM. The capacity of the line between buses 1 and 2 is 40 MW. Suppose the supply CB at bus 2 is fixed at 0.1 MWh. Fig. 4.3 shows the probability distribution for the *rate of convergence* between the DAM and RTM prices, where a negative value indicates price divergence. The rate of convergence is the price gap *before* and *after* the presence of the CB. In this example, *price convergence* occurs at 70% probability and *price divergence* occurs at 30% probability.

4.2 Anomaly Detection in IoT-Based PIR Occupancy Sensors to Improve Building Energy Efficiency

Energy demand in buildings currently accounts for 40% of the total U.S. energy consumption [60]. This calls for efforts to make buildings more energy-efficient. In this regard, smart buildings are receiving growing attention with the integration of building energy management systems (BEMS) and the proliferation of Internet-of-Things (IoT) [61–63]. An IoT-based BEMS may include hundreds of IoT devices, such as sensors, actuators, and communications nodes. These IoT devices monitor and control various load components, such

as lighting, heating, ventilating, and air conditioning (HVAC), and plug-in loads. The IoT sensors produce a huge amount of data streams, which can provide new opportunities to enhance energy efficiency in buildings.

In this section and its corresponding paper in [56], we analyze the *real-world* data streams that come from a recent IoT-based BEMS deployment in a large-sacle 101,670 sqft academic building at California State University, Long Beach with over 1000 IoT devices, which provide high granular monitoring and control capabilities for lighting, plug-in loads, and HVAC loads. Specifically, we look into the data from hundreds of digital passive infrared (PIR) occupancy sensors that are integrated into each lighting fixture in this building. All lighting fixtures have LED lights as well as integrated wireless communications capabilities. Note that, each room is equipped with tens of such IoT-based PIR occupancy sensors, which provide us with the occupancy status of each covered area within the room.

Our goal in this section is to detect anomalies in such real-world data streams from PIR sensors and to subsequently use the results to enhance energy efficiency in the building and open up opportunities to offer demand response services.

4.2.1 Introduction

Literature Review

There are few studies that have addressed the challenges related to anomaly detection in data streams from IoT devices in smart buildings. In [64] a new pattern-based anomaly classifier, the collective contextual anomaly detection using sliding window (CCAD-SW) is proposed to identify anomalous consumption patterns. In [65,66], anomaly

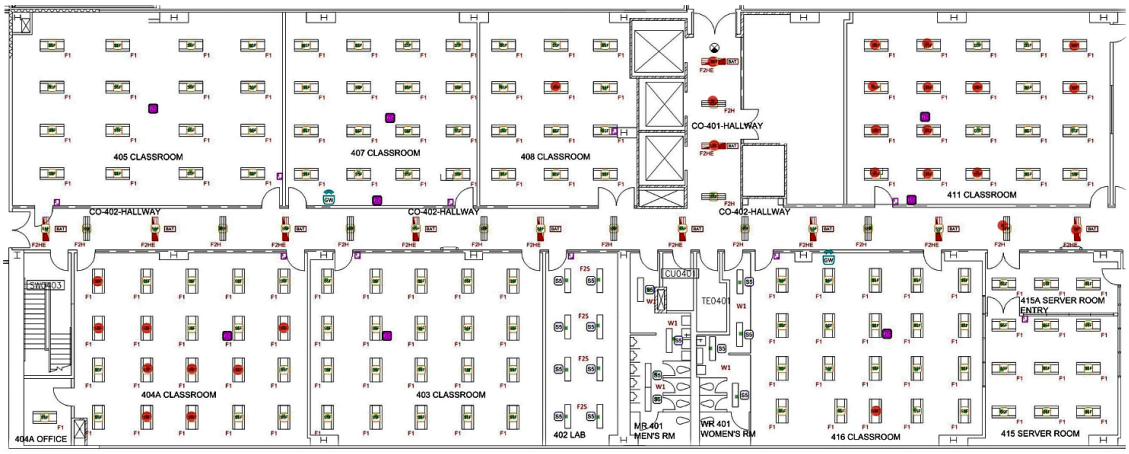

Figure 4.4: The layout of the fourth floor at the test site and the locations of the lighting fixtures and their integrated PIR occupancy sensors.

detection based on methods such as fuzzy linguistic description and nearest neighbor clustering is used to improve state-awareness and the understandability of BEMS data. In [67], a rule-based method is presented to detect energy inefficiencies in smart buildings. In [68], the design and implementation of a presence sensor platform is discussed that can be used for accurate occupancy detection at the level of individual rooms. There are also some papers, such as [69–71] that address the broad topic of energy efficiency issues in smart buildings, and some other papers, such as in [72–74], that address energy consumption prediction in smart buildings. All of the above papers are one way or another related to this study; however, none of the previous papers have addressed anomaly detection in IoT-based lighting-fixture-integrated PIR occupancy sensors; and application to energy saving and demand response. Moreover, most prior studies are not based on real-world data, as opposed to this study that is fundamentally a data-driven study built upon large volume of real-world data points.

Summary of Contributions

The contributions in this study are summarized as follows:

1. A two-step algorithm is proposed to find anomalies in occupancy data. In the first step, a factor showing the reliability level of each IoT lighting sensor is defined by using historical data. In the second step, real-time data is analyzed to find possible anomalies, which result in energy loss due to incorrect lighting system operation.

2. The application of the proposed two-step anomaly detection is presented for energy saving in smart buildings. Based on the forecasted amount of such energy saving under the proposed method, the under-study building can efficiently participate in demand response programs.

3. The forecasting component is built upon a deep neural network architecture based on long short-term memory (LSTM). We show that this deep learning algorithm can forecast the power consumption with high accuracy.

4. The analysis in this study is based on real-world data from hundreds of PIR sensors at the test site. A total of 2,088,170 data points are analyzed in this study. Our estimated energy saving in the lighting system is 30%.

4.2.2 Problem Statement

The focus in this section is on explaining the problem we are facing in a real-world R&D project. The test site for this project is a large six-story academic building with

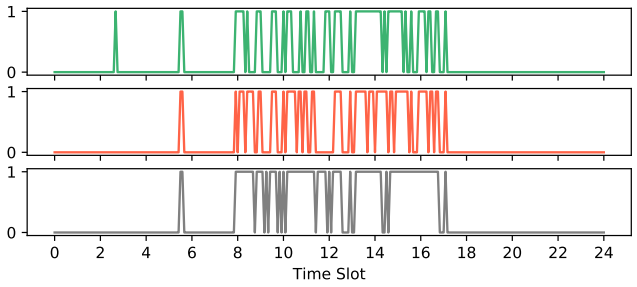

Figure 4.5: An example daily output for three PIR sensors in room 408.

hundreds of LED lighting fixtures. Each lighting fixture is equipped with a PIR occupancy sensor. As an example, the layout of the 4th floor and the location of the lighting fixtures are shown in Fig. 4.4, [75]. It should be noted that this building is equipped with three types of IoT devices, lighting, HVAC and plug-in load control; however, only the lighting system is the focus of this study.

As an example regarding the type of data that is available for this study, Fig. 4.5 shows the daily output for one day for three PIR occupancy sensors in room 408. Note that, this room has 12 lighting fixtures, which provides 12 separate data streams, one for each PIR occupancy sensor. The reporting interval of each sensor is 5 minutes. Therefore, each sensor provides 288 data points per day. Each reading is either 1, indicating "Occupied", or 0, indicating "Not Occupied".

Currently, the lighting control system is set to work as follows: In each room, if any of the PIR sensors at any lighting fixture within that room detects occupancy, lights automatically turn on. Also, lights automatically turn off if none of the PIR sensors at any lighting fixture within that room detect occupancy for a duration of 5 minutes.

Given the above setup and the availability of the real-world data streams, we seek to answer the following questions: 1) Is the data coming from each PIR sensor at each lighting fixture reliable? For example, could it be that there is no one in a room, yet one or more of the PIR sensors incorrectly detect occupancy? 2) If the answer to the first question is Yes, then how can we detect such anomaly? 3) How should we take action on such finding, i.e., how should we incorporate such indication into the existing lighting control system? 4) How can we enhance the demand response capability of the lighting loads in this process? Note that, in general, anomalies may have different causes, such as sensor failure, improper setting of sensors, communications issues, or even cyber-attacks.

4.2.3 Proposed Methodology

Anomaly Detection

For each room, let m denote the number of PIR sensors. At each reading interval t, let $\delta[t, i]$ denote the reading of PIR sensor i, where $i = 1, \ldots, m$. The number of triggered sensors, i.e., those that return 1 as their output, is obtained as

$$N[t] = \sum_{i=1}^{m} \delta[t, i]. \tag{4.1}$$

First, we consider the output of the PIR sensors as *suspicious* if $N[t]$ is smaller than a certain threshold N_{th}. In particular, based on our experience in manually investigating the data streams in this project, we set the threshold to be $N_{\text{th}} = 2$, i.e., when only one or at most two PIR sensors detect occupancy. Other values could also be considered for this threshold.

Next, we define a reliability index for each PIR sensor i, as

$$S[i,t] = \sum_{\tau=0}^{T} b[i, t-\tau], \tag{4.2}$$

where

$$b[i,t] = \mathbb{I}\left(\delta[i,t] = 1 \mid N \leq N_{\text{th}}\right). \tag{4.3}$$

Note that, $b[i,t]$ indicates whether the PIR sensor i was a *cause* of the suspicious observation in the readings of the PIR sensors in this room at time interval t. As for the reliability index $S[i,t]$, it indicates whether the behavior observed from PIR sensor i under such suspicious condition was *persistent* or *momentary*. Note that, T is a parameter with respect to how far back in time we would like to check the operation of the sensor in order to obtain its reliability index. This parameter is set based on the knowledge of the expert operator of the building and also the available history record of sensors, such as the information on whether there was any maintenance or if the sensor was replaced or calibrated recently.

By keeping track of $S[i,t]$, it shows the reliability of each sensor, and whether the suspicious observation $N \leq N_{\text{th}}$ should indeed be declared as anomaly. In this regard, next, we define two thresholds with respect to $S[i,t]$, namely $S_{\text{th,min}}$ and $S_{\text{th,max}}$. Specifically, on one hand, if $S[i,t] > S_{\text{th,max}}$, then the suspicious observation $N \leq N_{\text{th}}$ was *persistent* to be caused by sensor i, suggesting that it is likely an anomaly and the room is likely not occupied. On the other hand, if $S[i,t] < S_{\text{th,min}}$, then the suspicious observation $N \leq N_{\text{th}}$ was *momentary*, suggesting that it is likely an unusual but valid occupancy pattern and the room is indeed occupied. As for the third case, where the following inequalities hold: $S_{\text{th,min}} \leq S[i,t] \leq S_{\text{th,max}}$, then we must check time interval t before we make a final conclusion, as we explain next.

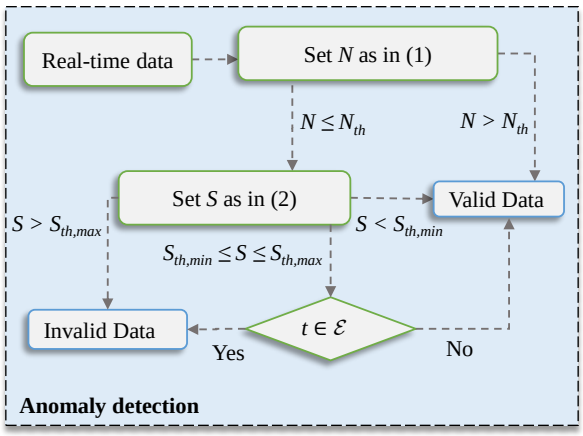

Figure 4.6: Outline of the proposed anomaly detection method.

Suppose $\mathcal{E}$ denotes the time slots during which the room is empty in normal circumstances. For example, for a classroom, we can check the class schedule, and set $\mathcal{E}$ to include the time slots from mid-night till 4:00 AM; or any other time frame(s). If $t \in \mathcal{E}$, when we know that the building is normally empty, thus, the observation is likely to be an anomaly; otherwise, it is treated as an unusual but valid occupancy. Parameters $S_{\text{th,min}}$ and $S_{\text{th,max}}$ can be set based on experiments and historical data. We set $S_{\text{th,min}} = 1000$ and $S_{\text{th,max}} = 2000$.

The outline of the proposed anomaly detection method is shown in Fig. 4.6. It takes in real-time data and detects possible anomalies, going through the steps that we explained above.

Potential for Energy Saving

Recall from Section II that the lighting control system is set in a way that triggering even one of the PIR occupancy sensors in a room results in turning on the lights in that room. In this regard, the proposed anomaly detection method can detect faulty or highly sensitive sensors which cause an anomaly for the lighting system in the room, i.e., unnecessarily turning on the lights. Therefore, having accurate occupancy data can help in saving energy in different parts of the building. Note that, since the purpose of this study is to enhance energy saving, we only address faults that cause unneeded energy usage. Since there is major overlap in the coverage areas among the PIR sensors in each room, there is redundancy in detecting occupancy. In fact, in our experiments, it has never happened that someone enters the room and none of the sensors pick it up. Therefore, a potential fault to miss occupancy is not a practical concern in this study and we do not address it.

Specifically, in the real-time operation of the BEMS, if an occupancy data is considered as anomaly based on the proposed method, the lights in the room should *not* be turned on. This can result in a major amount of energy saving. Consider a faulty or highly sensitive sensor in a room. This single faulty sensor can turn on the lights in a room all day and night, regardless of the operation of the rest of the occupancy sensors in that room. In fact, without considering the proposed method, certain components of smart buildings, such as certain rooms, may even result in more energy loss than conventional buildings. The difference in energy consumption between utilizing our proposed method and operating the system as is, i.e., ignoring the possible anomalies, is the amount of the energy that can saved when our method is implemented.

Demand Response and Energy Forecasting

The proposed anomaly detection method can be used also to create new capacities for the lighting control system to participate in demand response programs. The key is to adjust the parameters of the algorithm, i.e., N_{th}, $S_{\text{th,min}}$, $S_{\text{th,max}}$, T, and $\mathcal{E}$, under demand response operating conditions. That is, while the parameters can be set conservatively for energy saving during normal operating conditions; they can be set rather aggressively during demand response events. For example, we may set $N_{\text{th}} = 2$ during normal operating conditions, so that we check for anomaly if fewer than two PIR sensors are triggered. During a demand response event, we may change this to $N_{\text{th}} = 3$, so that we turn off the lights more aggressively when we observe potential faulty sensors. This opens up addition load reduction capacities that can we used during the demand response events. Such adjustments can be done also based on the location of the sensor, such as whether it is close to a door or a window, again based on the knowledge and experience of an expert operator for the understudy building.

Consider a "Basic Plan", which does *not* use the proposed anomaly detection method. Based on the actual historical data from the lighting fixtures, we train an LSTM model, which is a Recurrent Neural Network (RNN) [76], see Fig. 4.7. The trained LSTM model can predict the day-ahead energy usage of the lighting fixtures based on historical data. Next, consider a "Demand Response Plan" which uses the proposed anomaly detection method for any given choice of parameters. This time, we apply the anomaly detection method to historical data and train a second LSTM model to predict the day-ahead energy usage when the anomaly detection method is utilized.

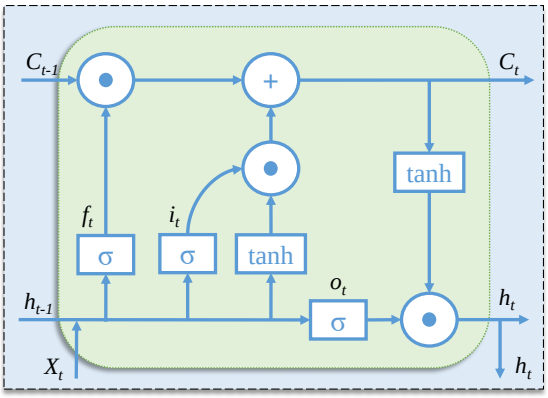

Figure 4.7: Architecture of an LSTM cell that is used for load forecasting.

Given the two prediction models, the *difference* between the Basic Plan and the Demand Response Plan is calculated to obtain the overall *predicted demand response capacity*. Such prediction is then reported to the demand response aggregator, as the amount of load reduction that we expect to be able to provide, in case a demand response event occurs.

Once the demand response mode is activated, the building operation is set such that the lights in each room do not turn on when *both* of the following conditions happens: 1) an anomaly is detected for the PIR occupancy sensors in that room; and 2) a demand response event occurs. In other words, we utilize the potential for energy reduction only during the demand response events. Again, the two prediction models are used in order to estimate the amount of available energy reduction, i.e., the demand response capacity, which is needed in order to participate in most practical demand response programs [77].

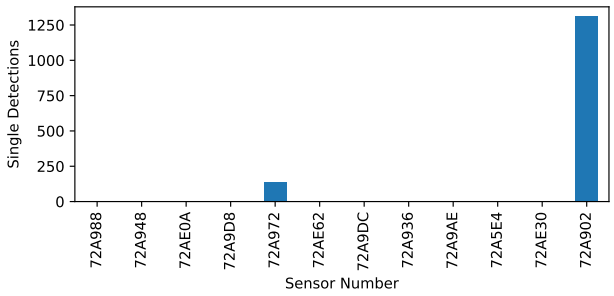

Figure 4.8: Number of single detections for each sensor in room 408.

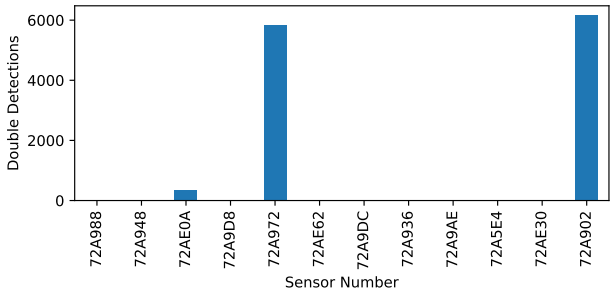

Figure 4.9: Number of double detections for each sensor in room 408.

4.2.4 Case Studies

In this section, we evaluate the performance of the proposed anomaly detection method using real-world data. It should be noted that while the data is real, the calculation of the energy saving is done numerically. The data contains the motion detection output of each sensor and the energy usage of its fixture. The analyzed historical data is for 45 days. We focus on the 4th floor of this building and it should be mentioned that corridors are excluded in this analysis due to safety.

Anomaly Detection

Based on the proposed anomaly detection method, in the first step, we determine the reliability level for each sensor in each room. As an example, Fig. 4.8 and Fig. 4.9 depict the number of single and double detections, respectively, in room 408. As we can see, sensor 72A902 with 1313 single detections and 6169 double detections and also, sensor 72A972 with 138 single detections and 5845 double detections over 12970 time slots are two unreliable sensors in this room. Any suspicious detection with $N \leq 2$ corresponding to these two sensors will be considered as anomaly and the reported data is invalid. Note that, these two sensors are not close to each other.

Energy Usage Forecasting

Based on what explained in the previous section, valid and invalid occupancy detections will be separated in the historical data. For the invalid occupancy data, as we determined that room as unoccupied, the energy consumption of that room at that time will be considered as zero. Accordingly, there are two time series for energy consumption. One with modifying the data based on the proposed anomaly detection method and the other one without utilizing our proposed method. The amount of energy usage *with* and *without* employing the proposed method in the under-study period is 1.4626 MWh and 2.0633 MWh, respectively. Therefore, by utilizing this method energy usage reduces by about 30%, which is a significant amount.

In the forecasting part, we utilize LSTM to train a model for the power consumption time series. As mentioned before, this is a day-ahead forecasting and in order to

forecast the power consumption of each time step, the model utilize the data for the days in the previous week. Note that as we are working on an academic building, only weekdays are taken into consideration. In order to train the model, the historical data is split into training and testing data sets. The first 80% of the data is used for training and the last 20% for testing the model. Fig. 4.10 shows the forecasted and the actual power consumption in the test data by utilizing the proposed method. The accuracy of this prediction model for the training and testing datasets is 85% and 84%, respectively.

Fig. 4.11 shows the forecasted and actual power consumption in the test data for the unmodified data. The accuracy of this model for the training and testing datasets is 73% and 72%, respectively. By comparing Fig. 4.10 and Fig. 4.11 , we can identify a biased power consumption in Fig. 4.11. This constant consumption is because of malfunction occupancy sensors, which result in unnecessary power consumption even at nights. Utilizing the proposed day-ahead forecasting model, we can forecast next day's power consumption and see how much it can save energy. Based on the day-ahead forecasted amount of energy saving, buildings can efficiently participate in demand response programs by having different override plans. Each plan will be constructed based on the proposed anomaly detection method by changing different parameters.

4.2.5 Conclusions

This study established an anomaly detection method for occupancy data from PIR sensors in IoT-based lighting systems, with application to building energy efficiency. First, based on historical data, suspicious sensors were identified at each room or zone. This

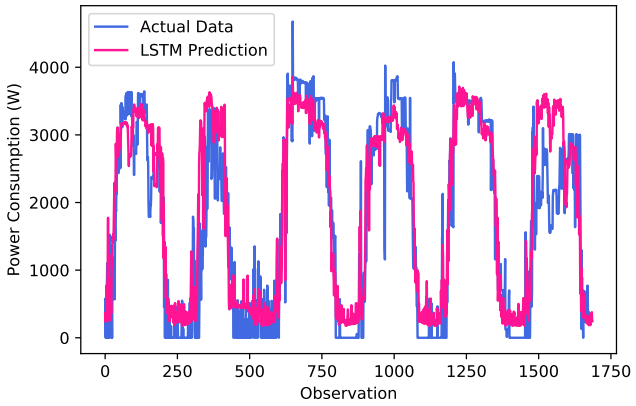

Figure 4.10: Actual and forecasted load with utilizing the proposed method.

identification was based on occupancy detections which were out of normal expectation. Next, real-time occupancy data were analyzed to distinguish between valid and invalid data. We analyzed the lighting system in a large academic building in California, which is equipped with such IoT-based network of PIR sensors. Our analysis shows that utilizing our proposed method can reduce energy consumption by about 30% in this building. By utilizing LSTM as a deep neural network architecture, the day-ahead energy consumption was forecasted so that the identified energy consumption reduction can be used to offer demand response. This study can be extended in various directions. In particular, our analysis can be done also on the HVAC and plug-in load controllers and the effect of anomalies in occupancy data on these systems can be investigated.

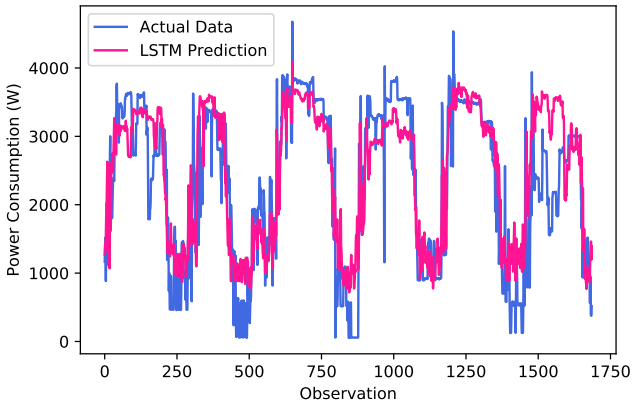

Figure 4.11: Actual and forecasted load without utilizing the proposed method.

Chapter 5

Conclusions and Future Work

In this dissertation, various aspects of convergence bidding in two-settlement electricity markets were analyzed.

A data-driven analysis of real-world electricity market data from the California ISO market was provided in this dissertation to *understand*, *reverse engineer*, and *enhance* the behavior of convergence bidders. It was discussed that a total of 20 CB market participants currently have a considerable presence in the California ISO that accounts for 72% to 84% of the entire CB market. The different bidding characteristics of these most present market participants were analyzed. Next, four quantitative features were extracted from all the submitted CBs; and by using the density based clustering algorithm, three main clusters of CB strategies were identified. The characteristics and the performance of each identified cluster of strategies were analyzed and some of their *advantages* and *disadvantages* were investigated. Two interesting discoveries were discussed. First, the Opportunistic Strategy does *not* match any of the convergence bidding strategies that currently exist in

the literature. Second, most papers in the literature are focused on the Self-Scheduling Strategy, while in practice, this strategy is *less* common among the market participants in the California ISO.

After reverse engineering the convergence bidding strategies of the real-world market participants in the California ISO market, a new comprehensive *composite* CB strategy was proposed. It was shown that the proposed strategy, optimally utilizes the advantages of various identified reverse engineered strategies under different market conditions. The new strategy was developed in three steps: First, by focusing on the Opportunistic Strategy as the newly discovered strategy, an optimization-based algorithm was proposed to maximize the total net profit of the market participant by capturing the price spikes. Second, an algorithm was developed to dynamically label each node based on the solution of the optimization problem in the first step. Third, by using the results from the first two steps for the Opportunistic Strategy, as well as by combining them with the Price-Forecasting Strategy and the Self-Scheduling Strategy, a strategy selection algorithm was proposed to complete a comprehensive composite CB strategy. It was shown in a case study that the annual profit of the most lucrative market participant could increase by over 40% if the proposed comprehensive strategy had been used.

Furthermore, the open problem of understanding the operation and impact of CBs during blackouts was addressed in this dissertation. A new functional method as well a new metric was introduced to determine if a cleared CB is exacerbating or healing the blackout. A series of mathematical theorems were developed and numerical analysis were conducted. It was shown that, when there is no congestion in the DAM, and even most often when there

is congestion in the DAM, supply CBs hurt the system during blackouts while demand CBs help the system. The impact of load shedding on the profit of CBs was also investigated in this study. The analysis in this part was again both analytical and numerical. It was shown that, load shedding usually creates advantage for supply CBs and disadvantage for demand CBs in terms of their profit. The combination of these various results raised the issue on whether the operation of CBs is fair and justified during the blackouts. Therefore, to gain more insights, we also analyzed the real-world market data from the California ISO during the blackouts in August 2020. It was shown that, the decision by the California ISO to suspend CBs during this event is justified and it matches the mathematical and numerical results that were obtained in this study.

The study in this dissertation can be extended in different directions. For example, we may investigate how the identified real-world CB strategies in Chapter 2 may positively or negatively affect price convergence and the efficiency of the electricity market. In other words, we may investigate the system-level impact of the identified real-world bidding strategy and/or the proposed composite bidding strategy. We may also analyze and reverse engineer the bidding strategy of the market participants that submit physical bids as well to understand and learn from their bidding strategies. Another interesting path for potential future research is to investigate the impact of the behavior of CB market participants on each other; i.e., by using concepts and methods in Game Theory. Furthermore, one can investigate and analyze the impact of convergence bidding on the blackouts that happened in Texas in 2021.

Bibliography

[1] U.S. Energy Markets 101: How Electricity Markets Work, [Online]: https://www.leveltenenergy.com/post/energy-markets-101.

[2] W. Hogan, "Virtual bidding and electricity market design," *The Electricity Journal*, vol. 29, no. 5, pp. 33–47, 2016.

[3] J. Parsons, C. Colbert, J. Larrieu, T. Martin, and E. Mastrangelo, "Financial arbitrage and efficient dispatch in wholesale electricity markets," *MIT Center for Energy and Environmental Policy Research*, 2015.

[4] M. Kohansal, E. Samani, and H. Mohsenian-Rad, "Understanding the structural characteristics of convergence bidding in nodal electricity market," *IEEE Transactions on Industrial Informatics*, vol. 17, no. 1, pp. 124–134, 2021.

[5] Defining convergence (virtual) bidding in California ISO, [Online]: https://www.caiso.com/Documents/ConvergenceBiddingSession1-DefiningConvergenceBidding.pdf.

[6] Virtual Transactions in the PJM Energy Markets, [Online]: http://www.pjm.com/media/documents/reports/20151012-virtual-bid-report.ashx.

[7] W. W. Hogan, "Revenue sufficiency guarantees and cost allocation," *Comments submitted to the Federal Energy Regulatory Commission, Docket No. ER04-691065*, 2006.

[8] J. Kazempour and B. F. Hobbs, "Value of flexible resources, virtual bidding, and self-Scheduling in two-settlement electricity markets with wind generation - part I: principles and competitive model," *IEEE Transactions on Power Systems*, vol. 33, no. 1, pp. 749–759, 2017.

[9] J. Kazempour and B. F. Hobbs, "Value of flexible resources, virtual bidding, and self-Scheduling in two-settlement electricity markets with wind generation - part II: ISO models and application," *IEEE Transactions on Power Systems*, vol. 33, no. 1, pp. 760–770, 2017.

[10] C. K. Woo, J. Zarnikau, E. Cutter, S. Ho, and H. Leung, "Virtual bidding, wind generation and California's day-ahead electricity forward premium," *The Electricity Journal*, vol. 28, no. 1, pp. 29–48, 2015.

[11] I. Mercadal, "Dynamic competition and arbitrage in electricity markets: The role of financial players", [Online]: http://home.uchicago.edu/~ignaciamercadal/IgnaciaMercadalJMP.pdf.

[12] R. Li, A. Svoboda, and S. Oren, "Efficiency impact of convergence bidding in the California electricity market," *Journal of Regulatory Economics*, vol. 48, no. 3, pp. 245–284, 2015.

[13] L. Hadsell, "The impact of virtual bidding on price volatility in New York's wholesale electricity market," *Economics Letters*, vol. 95, no. 1, pp. 66–72, 2007.

[14] W. Tang, R. Rajagopal, K. Poolla, and P. Varaiya, "Model and data analysis of two-settlement electricity market with virtual bidding," in *Proc. of the IEEE 55th Conference on Decision and Control (CDC)*, Las Vegas, NV, 2016.

[15] L. Hadsell and H. A. Shawky, "One-day forward premiums and the impact of virtual bidding on the New York wholesale electricity market using hourly data," *Journal of Futures Markets: Futures, Options, and Other Derivative Products*, vol. 27, no. 11, pp. 1107–1125, 2007.

[16] A. Jha and F. A. Wolak, "Testing for market efficiency with transaction costs: An application to convergence bidding in wholesale electricity markets," in *Industrial Organization Seminar at Yale University*, 2013.

[17] A. Jha and F. Wolak, "Can financial participants improve price discovery and efficiency in multi-settlement markets with trading costs?" National Bureau of Economic Research, Tech. Rep., 2019.

[18] J. Mather, E. Bitar, and K. Poolla, "Virtual bidding: equilibrium, learning, and the wisdom of crowds," *IFAC-PapersOnLine*, vol. 50, no. 1, pp. 225–232, 2017.

[19] J. Larrieu, "Impact of virtual bidding on forward premia in the California independent system operator," *Available at SSRN 2853596*, 2015.

[20] W. Tang, R. Rajagopal, K. Poolla, and P. Varaiya, "Impact of virtual bidding on financial and economic efficiency of wholesale electricity markets," Working paper, Tech. Rep., 2018.

[21] P. You, D. F. Gayme, and E. Mallada, "The role of strategic load participants in two-stage settlement electricity markets," in *Proc. of the IEEE Conference on Decision and Control (CDC)*, Nice, France, 2019.

[22] A. Long and A. Giacomoni, "Exploring the impacts of virtual transactions in the PJM wholesale energy market," in *Proc. of the IEEE PES General Meeting (PESGM)*, Montreal, QC, Canada, 2020.

[23] Convergence Bidding Definition, [Online]: https://www.caiso.com/Documents/ConvergenceBiddingSession1-DefiningConvergenceBidding.pdf.

[24] W. Ding, F. Zhang, Y. Zhelin, R. Liu, Y. Liu, and Z. Jing, "Supervision mechanism of virtual bidding in electricity market: a review," in *IOP Conference Series: Earth and Environmental Science*, vol. 675, no. 1. IOP Publishing, 2021, p. 012130.

[25] A. Isemonger, "The benefits and risks of virtual bidding in multi-settlement markets," *The Electricity Journal*, vol. 19, no. 9, pp. 26–36, 2006.

[26] M. Kohansal and H. Mohsenian-Rad, "Sensitivity analysis of convergence bids in nodal electricity markets," in *Proc. of the IEEE PES North American Power Symposium (NAPS)*, Morgantown, WV, Sep. 2017.

[27] S. Ledgerwood and J. Pfeifenberger, "Using virtual bids to manipulate the value of financial transmission rights," *The Electricity Journal*, vol. 26, no. 9, pp. 9–25, 2013.

[28] C. Lo Prete, N. Guo, and U. V. Shanbhag, "Virtual bidding and financial transmission rights: An equilibrium model for cross-product manipulation in electricity markets," *IEEE Transactions on Power Systems*, vol. 34, no. 2, pp. 953–967, 2019.

[29] J. R. Birge, A. Hortaçsu, I. Mercadal, and J. M. Pavlin, "Limits to arbitrage in electricity markets: A case study of MISO," *Energy Economics*, vol. 75, pp. 518–533, 2018.

[30] Y. Shan, C. Lo Prete, G. Kesidis, and D. J. Miller, "A simulation framework for uneconomic virtual bidding in day-ahead electricity markets," in *Proc. of the American Control Conference (ACC)*, Seattle, WA, 2017.

[31] D. Choi and L. Xie, "Economic impact assessment of topology data attacks with virtual bids," *IEEE Transactions on Smart Grid*, vol. 9, no. 2, pp. 512–520, 2016.

[32] A. Tajer, "False data injection attacks in electricity markets by limited adversaries: stochastic robustness," *IEEE Transactions on Smart Grid*, vol. 10, no. 1, pp. 128–138, 2017.

[33] M. Celebi, A. Hajos, and P. Hanser, "Virtual bidding: the good, the bad and the ugly," *The Electricity Journal*, vol. 23, no. 5, pp. 16–25, 2010.

[34] S. Baltaoglu, L. Tong, and Q. Zhao, "Algorithmic bidding for virtual trading in electricity markets," *IEEE Transactions on Power Systems*, vol. 34, no. 1, pp. 535–543, 2018.

[35] W. Wang and N. Yu, "A machine learning framework for algorithmic trading with virtual bids in electricity markets," in *Proc. of the IEEE PES General Meeting (PESGM)*, Atlanta, GA, 2019.

[36] D. Xiao, W. Qiao, and L. Qu, "Risk-constrained stochastic virtual bidding in two-settlement electricity markets," in *Proc. of the IEEE PES General Meeting (PESGM)*, Portland, OR, 2018.

[37] M. Kohansal, A. Sadeghi-Mobarakeh, S. D. Manshadi, and H. Mohsenian-Rad, "Strategic convergence bidding in nodal electricity markets: Optimal bid selection and market implications," *IEEE Transactions on Power Systems*, vol. 36, no. 2, pp. 891–901, 2021.

[38] D. Xiao, W. Qiao, and L. Qu, "Risk-averse offer strategy of a photovoltaic solar power plant with virtual bidding in electricity markets," in *Proc. of IEEE PES Innovative Smart Grid Technologies Conference (ISGT)*, Washington, DC, 2019.

[39] H. Mehdipourpicha and R. Bo, "Risk-constrained bi-level optimization for virtual bidder bidding strategy in day-ahead electricity markets," in *Proc. of the IEEE PES General Meeting (PESGM)*, Montreal, QC, Canada, 2020.

[40] D. Xiao, J. C. do Prado, and W. Qiao, "Optimal joint demand and virtual bidding for a strategic retailer in the short-term electricity market," *Electric Power Systems Research*, vol. 190, 2021.

[41] E. Samani, M. Kohansal, and H. Mohsenian-Rad, "A data-driven convergence bidding strategy based on reverse engineering of market participants performance: A case of california iso," *IEEE Transactions on Power Systems*, 2021.

[42] E. Samani and H. Mohsenian-Rad, "A data-driven study to discover, characterize, and classify convergence bidding strategies in California ISO energy market," in *Proc. of IEEE PES Innovative Smart Grid Technologies Conference (ISGT)*, Washington, DC, 2021.

[43] California ISO Open Access Same-time Information System, [Online]: http://oasis.caiso.com.

[44] Business Practice Manual for Definitions & Acronyms, v19, 2021 [Online]: https://bpmcm.caiso.com/BPM%20Document%20Library/Definitions%20and%20Acronyms/BPM_for_Defintions_and_Acronyms_V19_clean.docx.

[45] R. J. Campello, D. Moulavi, and J. Sander, "Density-based clustering based on hierarchical density estimates," in *Proc. of the Pacific-Asia Conference on Knowledge Discovery and Data Mining*, 2013.

[46] E. Samani and F. Aminifar, "Tri-level robust investment planning of DERs in distribution networks with AC constraints," *IEEE Transactions on Power Systems*, vol. 34, no. 5, pp. 3749–3757, 2019.

[47] I. Taheri, E. Samani, H. A. Abyaneh, H. Mohsenian-Rad, and A. Bakhshai, "A conceptual analysis of equilibrium bidding strategy in a combined oligopoly and oligopsony wholesale electricity market," *IEEE Transactions on Power Systems*, 2022.

[48] Master File Process, [Online]: http://www.caiso.com/CBT/MasterFileProcess/MasterFileProcess.html.

[49] S. Boyd and L. Vandenberghe, *Convex optimization*. Cambridge university press, 2004.

[50] Y. Fu and Z. Li, "Different models and properties on lmp calculations," in *Proc. of the IEEE PES General Meeting*, Montreal, QC, Canada, 2006.

[51] P. A. Ruiz, E. Goldis, A. M. Rudkevich, M. C. Caramanis, C. R. Philbrick, and J. M. Foster, "Security-constrained transmission topology control milp formulation using sensitivity factors," *IEEE Transactions on Power Systems*, vol. 32, no. 2, pp. 1597–1605, 2016.

[52] Power Systems Test Case Archive, [Online]: https://labs.ece.uw.edu/pstca/pf14/pg_tca14bus.htm.

[53] Final Root Cause Analysis Mid-August 2020 Extreme Heat Wave.pdf, [Online]: http://www.caiso.com/Documents/Final-Root-Cause-Analysis-Mid-August-2020-Extreme-Heat-Wave.pdf.

[54] PowerOutage.US, [Online]: https://poweroutage.us.

[55] California Independent System Operator Corporation Fifth Replacement FERC Electric Tariff, [Online]: http://www.caiso.com/Documents/Conformed-Tariff-as-of-Dec15-2021.pdf.

[56] E. Samani, P. Khaledian, A. Aligholian, E. Papalexakis, S. Cun, M. H. Nazari, and H. Mohsenian-Rad, "Anomaly detection in iot-based pir occupancy sensors to improve building energy efficiency," in *Proc. of IEEE PES Innovative Smart Grid Technologies Conference (ISGT)*, Washington, DC, 2020.

[57] Annual Report on Market Issues, http://www.caiso.com/Documents/2015AnnualReportonMarketIssuesandPerformance.pdf.

[58] National Renewable Energy Laboratory, [Online]: https://www.nrel.gov.

[59] Z. Taylor, H. Akhavan-Hejazi, E. Cortez, L. Alvarez, S. Ula, M. Barth, and H. Mohsenian-Rad, "Customer-side SCADA-assisted large battery operation optimization for distribution feeder peak load shaving," *IEEE Transactions on Smart Grid*, vol. 10, no. 1, pp. 992–1004, Jan. 2019.

[60] X. Cao, X. Dai, and J. Liu, "Building energy-consumption status worldwide and the state-of-the-art technologies for zero-energy buildings during the past decade," *Energy and buildings*, vol. 128, pp. 198–213, 2016.

[61] R. Jia, B. Jin, M. Jin, Y. Zhou, I. C. Konstantakopoulos, H. Zou, J. Kim, D. Li, W. Gu, R. Arghandeh *et al.*, "Design automation for smart building systems," *Proceedings of the IEEE*, vol. 106, no. 9, pp. 1680–1699, 2018.

[62] A. Al-Fuqaha, M. Guizani, M. Mohammadi, M. Aledhari, and M. Ayyash, "Internet of things: A survey on enabling technologies, protocols, and applications," *IEEE communications surveys & tutorials*, vol. 17, no. 4, pp. 2347–2376, 2015.

[63] D. Amaxilatis, O. Akrivopoulos, G. Mylonas, and I. Chatzigiannakis, "An iot-based solution for monitoring a fleet of educational buildings focusing on energy efficiency," *Sensors*, vol. 17, no. 10, p. 2296, 2017.

[64] D. B. Araya, K. Grolinger, H. F. ElYamany, M. A. Capretz, and G. Bitsuamlak, "An ensemble learning framework for anomaly detection in building energy consumption," *Energy and Buildings*, vol. 144, pp. 191–206, 2017.

[65] D. Wijayasekara, O. Linda, M. Manic, and C. Rieger, "Mining building energy management system data using fuzzy anomaly detection and linguistic descriptions," *IEEE Transactions on Industrial Informatics*, vol. 10, no. 3, pp. 1829–1840, 2014.

[66] O. Linda, D. Wijayasekara, M. Manic, and C. Rieger, "Computational intelligence based anomaly detection for building energy management systems," in *Proc. of the International Symposium on Resilient Control Systems*, Salt Lake City, UT, Aug. 2012.

[67] M. Peña, F. Biscarri, J. I. Guerrero, I. Monedero, and C. León, "Rule-based system to detect energy efficiency anomalies in smart buildings, a data mining approach," *Expert Systems with Applications*, vol. 56, pp. 242–255, 2016.

[68] Y. Agarwal, B. Balaji, R. Gupta, J. Lyles, M. Wei, and T. Weng, "Occupancy-driven energy management for smart building automation," in *Prof. of the ACM workshop on embedded sensing systems for energy-efficiency in building*, 2010.

[69] A. Allouhi, Y. El Fouih, T. Kousksou, A. Jamil, Y. Zeraouli, and Y. Mourad, "Energy consumption and efficiency in buildings: current status and future trends," *Journal of Cleaner production*, vol. 109, pp. 118–130, 2015.

[70] S. Ahmadi-Karvigh, A. Ghahramani, B. Becerik-Gerber, and L. Soibelman, "Real-time activity recognition for energy efficiency in buildings," *Applied energy*, vol. 211, pp. 146–160, 2018.

[71] B. Tan, Y. Yavuz, E. N. Otay, and E. Çamlıbel, "Optimal selection of energy efficiency measures for energy sustainability of existing buildings," *Computers & Operations Research*, vol. 66, pp. 258–271, 2016.

[72] P. A. Gonzalez and J. M. Zamarreno, "Prediction of hourly energy consumption in buildings based on a feedback artificial neural network," *Energy and buildings*, vol. 37, no. 6, pp. 595–601, 2005.

[73] J. Yang, H. Rivard, and R. Zmeureanu, "On-line building energy prediction using adaptive artificial neural networks," *Energy and buildings*, vol. 37, no. 12, pp. 1250–1259, 2005.

[74] M. Castelli, L. Trujillo, L. Vanneschi, and A. Popovič, "Prediction of energy performance of residential buildings: A genetic programming approach," *Energy and Buildings*, vol. 102, pp. 67–74, 2015.

[75] D. H. Tran, M. H. Nazari, A. Sadeghi-Mobarakeh, and H. Mohsenian-Rad, "Smart building design: a framework for optimal placement of smart sensors and actuators," in *Proc. of IEEE PES ISGT*, 2019.

[76] S. Hochreiter and J. Schmidhuber, "Long short-term memory," *Neural computation*, vol. 9, no. 8, pp. 1735–1780, 1997.

[77] H. Mohsenian-Rad and A. Leon-Garcia, "Optimal residential load control with price prediction in real-time electricity pricing environments," *IEEE Transactions on Smart Grid*, vol. 1, no. 2, pp. 120–133, 2010.